VEHICLE MOTIONS AS INFERRED FROM RADIO-SIGNAL-STRENGTH RECORDS

William C. Pilkington

JET PROPULSION LABORATORY
CALIFORNIA INSTITUTE OF TECHNOLOGY
PASADENA, CALIFORNIA

External Publication No. 551

VEHICLE MOTIONS AS INFERRED FROM RADIO-SIGNAL-STRENGTH RECORDS

William C. Pilkington

JET PROPULSION LABORATORY
CALIFORNIA INSTITUTE OF TECHNOLOGY
PASADENA, CALIFORNIA
September 5, 1958

ORDCIT Project
Contract No. DA-04-495-Ord 18
Department of the Army
ORDNANCE CORPS

External Publication No. 551

VEHICLE MOTIONS AS INFERRED FROM RADIO-SIGNAL-STRENGTH RECORDS

William C. Pilkington

Copy No._____
pp. ii-v, 1-91

JET PROPULSION LABORATORY
California Institute of Technology
Pasadena 3, California
September 5, 1958

CONTENTS

FIGURES

FIGURES (Cont'd)

FIGURES (Cont'd)

VEHICLE MOTIONS AS INFERRED FROM RADIO-SIGNAL-STRENGTH RECORDS[1]

William C. Pilkington[2]

ABSTRACT

The radio-signal-strength records from the Explorer satellites provided considerable information on staging, attitude, precession rate, spin rate, and ratio of moments of inertia. The records from the launching of each of the Explorers were investigated and gave information that could be used to explain the details of the performance. Records of later passes were used to determine the rate at which the cone angle of precession of the body increased and the time at which the body approached a tumbling motion. It is believed that radio-signal-strength records can be used in combination with other information to identify rocket vehicles, particularly after several similar vehicles have been received. The antenna patterns and transmitter frequencies of vehicles can be so designed that the removal of motional data from the records is much easier and more precise than it would be if this design factor had not been considered.

---

[1]This paper presents the results of one phase of research carried out at the Jet Propulsion Laboratory, California Institute of Technology, under Contract No. DA-04-495-Ord 18, sponsored by the Department of the Army, Ordnance Corps.

[2]Senior Research Engineer.

NOMENCLATURE

D = distance between antenna pattern nulls.

I_1 = pitch or yaw moment of inertia.

I_3 = roll moment of inertia.

R = distance of satellite from receiving station.

θ = half-cone angle of precession.

λ = wavelength.

$\dot{\varphi}$ = precession rate.

ω_3 = spin rate.

INTRODUCTION

Considerable data on various parameters of a satellite and its launching vehicle can be obtained from the received-signal-strength records at the various satellite receiver stations. The doppler shifts of the satellite can be used to determine the orbital characteristics quite accurately. (Ref. 1 discusses the rapid determination of these parameters.) Information concerning the velocity increment and direction of each stage can be obtained if doppler data are received by several stations during the high-speed staging. The variations in signal strength during launch can be used to find the spin rate of the satellite before, during, and after staging, and to find variations in attitude, including precession, during launch. With spin and precession frequencies available, any changes in the ratios of moments of inertia can be determined.

In this paper the launchings of the Explorer satellites will be used as a basis for the generalized conclusions concerning utilization of radio-signal-strength records. The discussion includes a description of the Explorer launching system.

THE EXPLORER LAUNCHING SYSTEM

The Explorer satellites were placed in orbit using a modified Jupiter C as the launching vehicle. The Jupiter C consisted of a modified Redstone missile as the first stage and three high-speed stages made up of clusters of small solid-propellant rocket motors.

The Redstone is a liquid-propellant rocket which was modified to form the first stage of the satellite-launching system. It was used

to carry the high-speed rocket stages and the orbiting payload to approximately the final orbital altitude. The Redstone also carried a special attitude control system and electric motors in an instrument compartment. The motors were used to spin the high-speed rocket assembly at about 12.5 revolutions per second. The attitude control system was needed to assure that the high-speed rockets were pointing correctly during firing of the second stage.

The high-speed stages were built from clustered solid-propellant rocket motors which had been developed for use in the testing of various solid fuels and motor geometries. The second stage consisted of eleven motors, the third stage consisted of three motors, and the fourth stage was a single motor on which was mounted the satellite payload. The entire assembly of the high-speed stages was carried inside a cylindrical structure. This cylinder was attached to a large shaft connected to the spin motors in the Redstone instrument compartment. The cylinder and motor assembly were spun at 12.5 rps to average out any one-sided thrust occurring during the burning of the high-speed stages. The clusters were fastened together by means of bulkheads. The stages were simply set one inside the other, and a series of launching lugs and sockets was used to maintain the close tolerances required for proper operation.

Figure 1 is a photograph of the Explorer III launching. It shows the Jupiter C missile, the cylinder, and the satellite. Figure 2 is a pictorial representation of a typical launching. The Redstone lifts the vehicle, and after burnout of the first stage, the instrument compartment containing the high-speed stages and the satellite separates and coasts. At approximately the peak altitude of the coast

the high-speed stages fire in sequence and the satellite is in orbit. The same launching system had been used earlier for carrying re-entry nose cones (i.e., nose cones which re-enter the atmosphere for recovery). The only significant difference was the absence of a fourth-stage motor in the earlier system.

EXPLORER SATELLITE INSTRUMENTATION

The instrumentation of the satellite launching system consisted of two distinct types. The instrument compartment of the first stage contained telemetry equipment to transmit to the launching area the various functions of the large liquid-propellant stage. This telemetry reported on many parameters including the attitude of the instrument compartment. The first-stage velocity was obtained by accurate two-way doppler (a radio signal was transmitted to the rocket vehicle, its frequency was doubled, and the signal was retransmitted to the ground where it was compared with the locally doubled version of the original signal).

The second, third, and fourth stages carried no telemetry for transmitting the performance of these stages. The rather small size of the satellite payload made it necessary to use all of the weight available for satellite instrumentation. The satellite transmitters, however, provided useful information on the functioning of the high-speed stages and on the attainment of a satisfactory orbit.

The Explorer satellite contained two stable RF oscillators, one at 108.00 mc and the other at 108.03 mc. In all the Explorers the 108.00-mc transmitter operated continuously. In Explorers II and III

the 108.03 transmitter operated only upon command. A more complete description of the instrumentation of Explorers I and III is contained in Appendix A.

The frequency stability of the beacons allowed determination of the doppler shift during the burning of the three high-speed stages. It could be easily determined whether or not all the stages had indeed burned and if approximately nominal performance had been obtained from them. With several receiving stations taking doppler records of the satellites on the launch phase, it was possible to construct a total velocity vector for the individual stages giving with reasonable accuracy the velocity increment of each stage and predicting to within a few degrees the angle at which each stage fired.

Each station recorded radio signal strength, and despite the problem of ionospheric disturbances, an analysis of these records was easily accomplished to determine the satellite spin rate and the presence or absence of significant precession or even tumbling of the satellite. After separation of the high-speed stages from the rocket launcher there was a long coast period in which the radio-signal-strength records allowed some determination of the proper performance of the attitude controller. The problems of separating ionospheric data from motional data were greatest in this portion of the records, since the period of signal-strength variations was not necessarily fixed, as it is in force-free precessional motion, by free rigid body mechanics.

At this point the various antenna systems will be briefly discussed. On Explorer I the 108.00-mc transmitter drove the nose cone of the satellite against the body of the satellite, thus forming a

short nonsymmetrical dipole. The nose cone was much shorter than the body of the satellite, and this produced a dipole-like antenna pattern with the maximum lobe bent toward the rear of the satellite to some extent. The 108.03-mc transmitter drove a turnstile-type antenna made up of four flexible whips attached to the body of the satellite. The whip antennas produced a circularly polarized antenna pattern with several decibels of ellipticity. The antenna patterns and a more complete description of this antenna system are presented in Appendix B. The patterns of the Explorer II satellite attempt were essentially identical to Explorer I.

The successful satellites Explorers III and IV had two dipole-type antennas. The 108.00-mc transmitter drove the front gap (the nose cone against the satellite body) as described for Explorer I, and the 108.03-mc transmitter drove another dipole-type antenna (the satellite body against the empty fourth-stage motor case). A description of this antenna system and the patterns for Explorer III, also applicable to Explorers IV and V, are presented in Appendix B.

DOPPLER DETERMINATION OF APPROXIMATELY CORRECT MOTOR FUNCTION

A single receiver located at or near the launch site can give approximate data on the velocity increment of each stage of the multi-stage vehicle in a very simple manner. Recording of the one-way doppler shift at this site allows comparison of the predicted doppler shift with the actual shift and thus provides a confirmation of proper operation.

Use of several stations at different locations allows by triangulation a relatively accurate determination of the actual velocity increment and direction of each high-speed stage. In the unsuccessful Explorer II it was easy to determine that stage 4 did not produce any change in the velocity vector. Motor failure is obvious. In Explorer III it was possible to determine from the doppler data that all motors fired but that the velocity vector was slightly in error in pitch but approximately correct in yaw. This angular error was confirmed by the low perigee.

ATTITUDE DATA

Fairly rapid changes in the attitude of the satellite vehicle can be found from signal-strength records, if the signal-strength variations due to this cause can be separated from the variations due to motor burning and those due to ionospheric conditions. Motor ignition and burning can produce variations in signal strength due to the high acceleration and vibration level, modifying the characteristics of the transmitter. Tests can be performed for this type of variation and the unit designed to minimize it. The variation in signal strength due to the ejection of burning gases and their modification of the transmitted signal cannot be avoided unless a receiver can be located specifically to minimize it, but estimates can be made; and, of course, motor burning is only a very small portion of the total period of interest.

The ionospherically induced variation in signal strength can be estimated and eliminated from the signal, particularly if people

skilled in ionospheric data are available, if data obtained by ionospheric instruments at the time of interest are available, and if the unit contains frequencies widely enough separated to allow use of the fact that Faraday rotation is proportional to the wavelength squared (λ^2). None of these conditions was fulfilled in the Explorer shots. However, during the coasting and staging of the vehicles, any rapid changes of the missile axis amounting to more than a few degrees can be easily noted.

SPIN DETERMINATION

The spin rate of the satellite vehicle about its long axis was fairly easy to determine, particularly during launch, and the principal receiving site looked toward the rear of the missile. The antenna pattern of the satellite transmitters was not perfectly symmetrical about the axis of rotation of the body; therefore, variation of signal strength at the spin rate was fairly easily read from the records. However, as the distance from the satellite-launching vehicle to the receiving station increased, noise obscured the spin record at various times. The various noise problems, including signal-strength variations during missile burning, also obscured the data on some records. However, on the four Explorer launchings in general, a variation of the signal strength at the spin rate, normally programmed to 12.5 rps, was clearly identifiable.

Included in this paper are four Figures (Figs. 3-6) which show the spin rate vs time near the time of injection; that is, the time when the last motor burned out. These four Figures are concerned with the

time from the coasting period just before the ignition of the stage 2 motor until some seconds after injection. Wherever the data is not clear, dotted lines are used to give an estimate of what could have occurred. The solid lines imply reasonable confidence in the accuracy of the data. Figure 3 is the record from the Explorer I launch. It will be noted that during the coasting period the spin was 12.5 rps as programmed. Stage 2 ignition apparently did not change this spin rate. During the coast after stage 2 burning, however, the rate was found to be approximately 12.3 rps, and during the burning of stage 3, points at 12.4 and 12.6 rps are found. The single point during the coast after stage 2 burning makes it necessary to estimate what happened during stage 2 burning and coast. The single point would not allow an indication that any change had occurred in the spin rate. However, the points during stage 3 burning strongly implied that some change did occur; and therefore a dotted line has been drawn from the known data in stage 2 down to approximately 12.3 rps, and then this rate is held constant during coast, as there is no mechanism for a change in spin rate during the coasting period, barring a catastrophic occurrence which we know could not have occurred here. During the burning of stage 3 the spin rate apparently increased from approximately 12.3 to approximately 12.6 rps. After the burnout of stage 3 this was approximately constant until ignition of stage 4. Upon ignition, probably through some mechanical process during separation of the stages, the rate suddenly dropped from approximately 12.6 down to approximately 10.6 rps. The rate then climbed slowly until at the burnout of stage 4 the rate was 11.1 rps. Several good points are available right after the burnout of this stage. A very interesting

event then happened which is to date unexplained in detail. The spin rate suddenly decreased from approximately 11.1 to approximately 9.5 rps. At the same time that the spin rate decreased, the amplitude of the modulation due to spin greatly increased and a change in signal strength occurred Figure 4 is a reproduction of a portion of this record. It is almost certain that some portion of the missile or antenna system moved in such a way as to change the ratio of the moments of inertia of the body so as to reduce the spin and change the antenna pattern of the vehicle at this point. The rate of spin then remained constant until the end of reception on this pass. On the next pass at this station the spin had significantly decreased. Further comments on the decrease of spin over the long period will be contained in the next portion of this report.

Figure 5 is a plot of spin for Explorer II over about the same period as the data discussed for Explorer I. The data during the Explorer II launch were not quite as easily read. During the coasting period prior to stage 2 ignition, the spin was approximately 12.3 rps or slightly below the programmed value. The next available data is just after stage 2 ignition, at which time the signal was very noisy, but two readings were obtained which implied that the spin might have increased to as high as 13.7 rps. No more data are available until the coast period after stage 3 burning. The dotted line which shows decrease only during stage 3 burning is based on the fact that short-term change cannot occur normally during the coast period. At the time when fourth-stage ignition should have occurred, a change in the reception was noted but no change in the velocity vector was found. It is therefore believed that the stage 4 motor misfired. The spin

remained constant throughout the rest of the time this vehicle was received. Without the velocity increment from stage 4, the vehicle of course did not go into orbit.

The spin data on the Explorer III launch is contained in Fig. 6. Note that the spin rate was approximately 12.7 rps during the entire coast period. Stage 2 ignition did not change the spin rate; it was continuous through stage 2 burning and stage 2 coast at 12.7 rps. No points were available during the stage 3 burning, but a good point is available during the coast period between stage 3 burnout and stage 4 ignition. The dotted line shows a rapid decrease on stage 3 ignition, but the spin could have varied in several other ways. At stage 4 ignition the spin apparently decreased to approximately 10 rps. One fairly poor point just after the start of burning gave a value of 9.8 rps. After burnout many points are available at 10 rps. The rate did not change during the rest of this record. Explorer III had no transient similar to that of Explorer I, and Explorer III went successfully into orbit, although there was a small angular error on injection (end of burning of stage 4).

The spin record of the Explorer IV launch phase is shown in Fig. 7. The spin was constant at 12.5 rps during the coasting phase before stage 2 ignition. Upon stage 2 ignition the spin remained sensibly constant and only changed upon ignition of stage 3. Several points imply that the spin changed from approximately 12.5 to about 11.9 rps at stage 3 ignition and remained relatively constant during the burning of stage 3 and the coast following it. Upon ignition of stage 4 the spin decreased to approximately 10.5 rps and then increased slowly to approximately 11.2 rps at the burnout of stage 4.

The spin then remained constant to the end of the launch pass. The reasons for the apparent decreases upon ignition are not completely understood, nor are the exact reasons for the increase during the burning understood. However, it is certainly easy to visualize possible reasons for each of these. An example of a reason for decrease might be some interference on the launching apparatus as the stages separate. A possible reason for the slow change during burning is the following: the gases going out of the nozzle have angular velocity relative to the nozzle since the radius at which the gases are generated is different from the nozzle radius, and this transfers angular momentum to the nozzle, changing the spin of the stage.

PRECESSION OF THE SATELLITE

Precession is defined here as a motion of the symmetry axis of a body. The axis of a torque-free symmetrical body in general traces out a cone. The method of determining the precession rate and the rate of increase of the cone angle of precession of satellites will be illustrated using Explorer III as an example. It should be pointed out that the Explorer satellites did not fulfill the conditions conducive to the easy separation of ionospheric data from data due to the motions of the vehicle. Some of the reasons for this were noted under the section titled Attitude Data. Appendix C contains data concerning the motions of vehicles in space and should be referred to if questions arise during the following discussion.

Figure 8 shows the major long-term signal-strength variation at the launch receiver during the launch pass of the Explorer III

satellite. This record, taken from the continuously transmitting 108.00-mc transmitter, shows a rather periodic variation of signal strength during the coast phase before ignition of the second, third, and fourth stages. It is likely that the variation noted is ionospheric data rather than motional data. However, assuming for the moment that it was motional data, one can use the antenna pattern and the approximate look angle (angle from missile symmetry axis to receiver) at this point and estimate that the total angular motion of the vehicle would be approximately 10 deg. This would imply an error in the launch angle at ignition of the high-speed stages much larger than would normally be expected from this configuration. The final velocity of Explorer III did have an angular error of the same order as that estimated; however, it is still likely that the variations were due to the ionosphere, since it has been reported that other stations received the signals but with variations of a different period.

Immediately after the end of burning of stage 4 (injection) the record showed an amplitude variation of about 6 db with an apparent period of 8.6 sec. At this time the predicted look angle was about 28 deg. If it is assumed that the data are not ionospheric but motional, the antenna patterns can be used to find what the full cone angle of precession of the vehicle might be. With the predicted (for a perfect flight) 28-deg look angle, the antenna data indicated a full cone angle of precession of about 20 deg. Later data on the orbit of Explorer III implied that the vehicle had approximately a 6-deg upward error in the velocity vector. This would change the look angle to about 20 deg, in which case the full cone angle of

precession would be approximately 15 deg. It is interesting to note that the signal strength received at the time of injection is approximately -128 to -130 dbm; the predicted value is -122 dbm. The missile antenna pattern has a tail-on null, so that if the missile tilted up several degrees, the signal would get weaker as the look angle gets smaller. This agrees with the orbital conclusion that the missile was tipped up at the time of injection. If the precession angle is estimated from the very weak data noted above, a full cone angle of the order of 10 to 25 deg would be estimated.

Inspection of signal-strength records from various stations over a period of several days leads to the belief that at least the data after injection are not ionospheric, since the period of precession, as implied by the radio-signal-strength data, remains approximately 8.6 sec at each station. The angle of precession, as implied by signal-strength records at the various stations, increases, and after about 10 days Explorer III was very close to a full cone angle of 180 deg; that is, approximately tumbling.

Figure 9 shows one way in which the cone angle of precession may be estimated. If a precessing satellite passes a receiving station at a distance R and has an antenna with nulls off the nose and tail, it can be estimated from close examination of the signal-strength records when the nose of the satellite is pointing at the station on the approach and when the tail is pointing at the station after passing. Nose and tail can, of course, be reversed. The distance D and the distance R then can be used to give a rough estimate of the cone angle of precession.

On one record of signal strength taken at Earthquake Valley (a radio receiver site near San Diego, California) the conditions necessary for the determination described above were apparently satisfied. The time between the nulls due to looking at the nose and the tail during passage was approximately 1.5 min. The velocity was assumed to be approximately 300 miles/min and D, the distance between nulls, approximately 450 miles. The minimum slant range R, as determined from doppler data and from the satellite orbit, was approximately 150 miles. Since the time between nulls is approximate, it can be said that the tangent of the half cone angle of precession is equal to 2R/E. The tangent of θ, therefore, equals 300/450 and θ equals approximately 34 deg. Thus, the full cone angle was approximately 68 deg at 47 hours after launch.

Inspection of another record at Earthquake Valley 5 days after launch reveals a similar situation. The range R was 195 miles by doppler, and the time between deep nulls was 1.0 min; therefore, the tangent equals 390/300, and thus $\theta = 52$ deg. The full cone angle was therefore 104 deg approximately 5 days after launch. Ten days after launch another Earthquake Valley record showed the null positions, which in this case were not too clearly defined. But the time between nulls was approximately 65 sec, and the range was approximately 420 miles. The distance D was approximately 320 miles, and the tangent equals 840/320. Thus, the full cone angle was 138 deg 10 days after launch. Curve 1 of Fig. 10 shows a plot of the points just described.

The cone angle of precession may also be obtained from rigid body mechanics and the spin and precession rates. The equation which is useful in obtaining precession cone angle is

$$\cos \theta = \frac{\frac{\omega_3}{\dot{\varphi}}}{\frac{I_1}{I_3}}$$

where ω_3, $\dot{\varphi}$, I_1, and I_3 are respectively the spin rate, the precession rate, the pitch or yaw moment of inertia, and the roll moment. Theta is the half angle of the precession cone. The moments were measured by a pendulum experiment using a duplicate of Explorer III. The ratio of moments measured was 82. The value of $\omega/\dot{\varphi}$ shortly after burnout has been measured from radio intensity variations and found to be 86. The agreement of radio and moment of inertia data is not sufficient to allow any θ estimate at injection. But if the spin rate and precession rate are measured vs time in days, these values may be inserted in the equation and will give a value of precession cone angle vs time. Precession rate is constant (this agrees with Eq. C-6 in Appendix C). Spin rate for Explorer III is plotted in Fig. 11.

It is seen that the spin rate slowly declines from approximately 10 rps down to approximately 2 rps at the end of 10 days. When this variable spin rate and the constant precession rate are inserted in the formula mentioned earlier, curve 2 on Fig. 10 results. The agreement between these two curves in Fig. 10 is not perfect, but it is reasonably good considering the number of points used and the basic quality of this type of data.

Two other methods of obtaining data from the radio-signal-strength records of a vehicle can be very useful for the same purposes discussed earlier. The first method is possible only if the body has two transmitters. If the antenna patterns of these two transmitters

have their maxima in different directions and have slopes typical of antenna patterns (slope varies with look angle), then the received-signal variations due to precession will be different for the two frequencies, and the look angle and the precession cone angle can be determined. The second method is applicable to a vehicle with only one transmitter. The signal-strength variations due to spin must be accurately known and must vary significantly with the look angle. A simple analysis of the signal-strength record then allows determination of spin rate, look angle, and precession cone angle.

From the methods discussed and the examples given it can be shown that with a minimum effort spent on interpreting the radio-signal-strength variations of a body in orbit, one can find several interesting facts about the free-body motions of this device. Appendix C contains a fairly complete analysis of the motions of a free body and an analysis of the motions of the Explorer I payload.

The signal-strength records for the Explorer IV launch are given in Fig. 12. No analysis of the motions of this device will be made, but apparently Explorer IV also approached a full cone angle of 180 deg, or tumbling, in 8 to 10 days. The period of precession of Explorer IV was approximately 6.5 sec. Explorer II did not go into orbit, so no determination of the time to full cone angle was undertaken. Explorer I, which had a slightly different configuration due to whip antennas (analyzed in Appendix C), apparently went into full cone angle of precession within very short period after launch, probably after approximately one orbit.

The launch signal-strength records for Explorers I and II are included as Figs. 13 and 14. No analysis is made, but the records are available for comparison with the other records discussed in some detail.

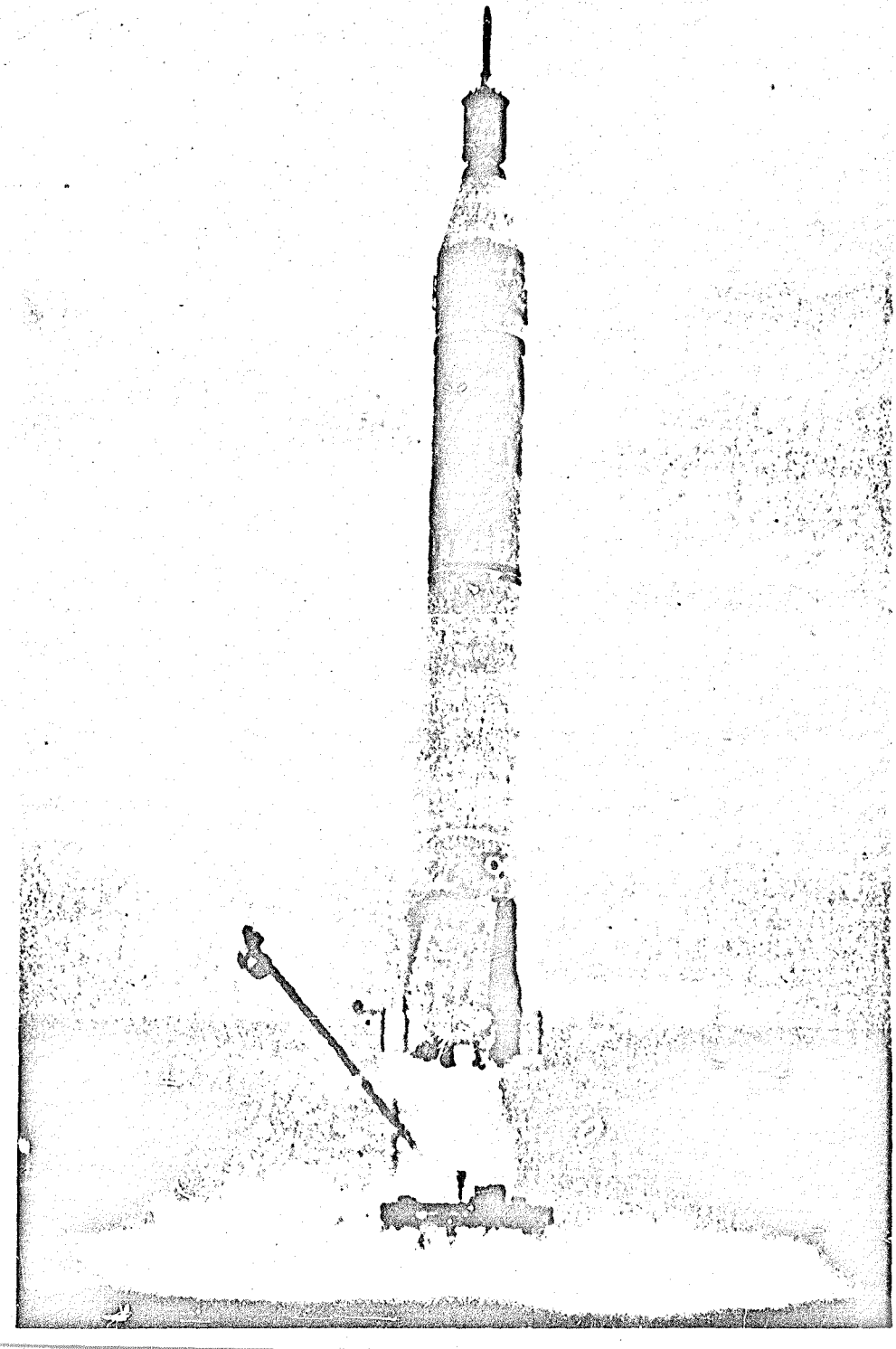

Fig. 1. Photograph of Explorer III Launching

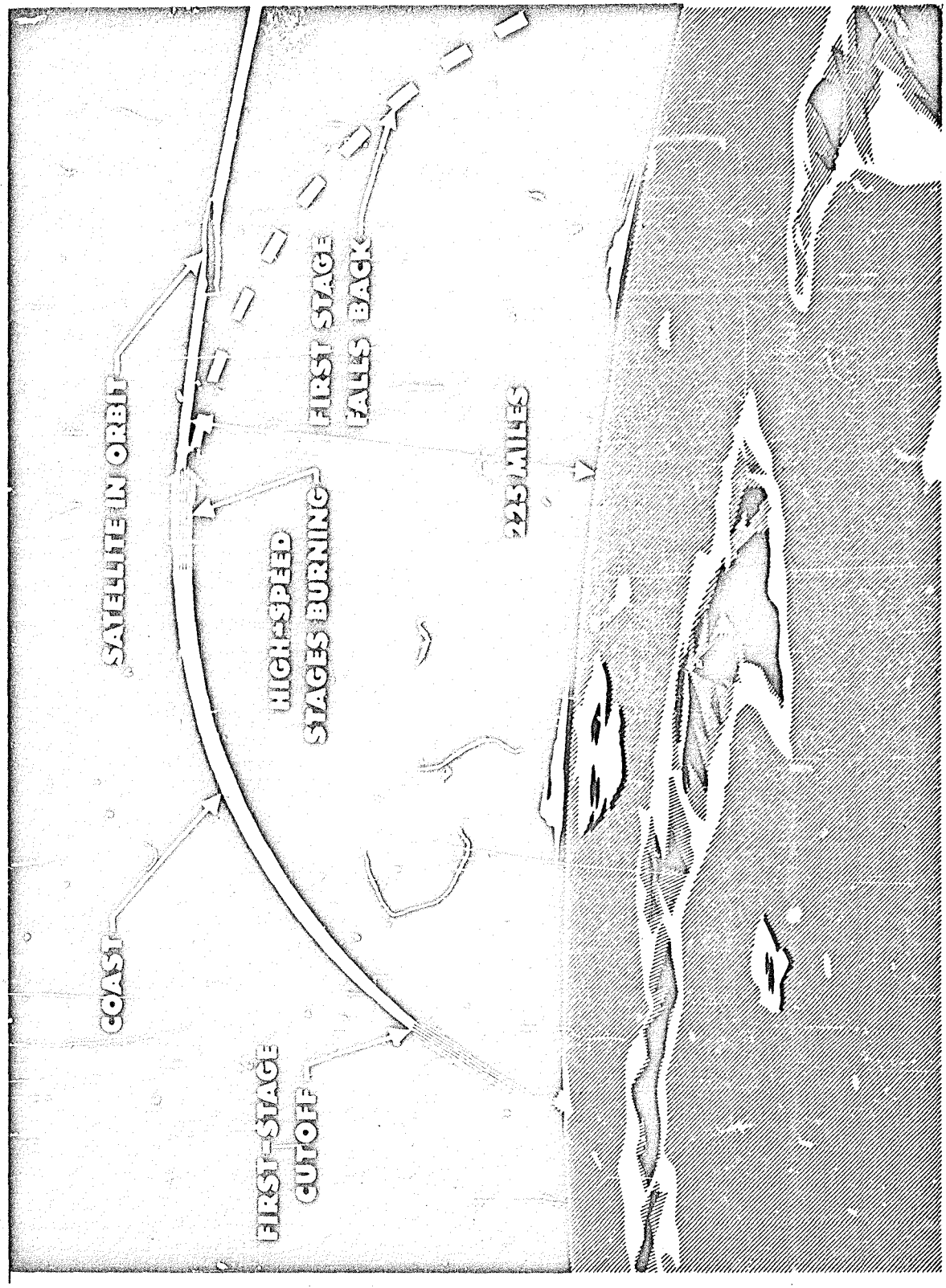

Fig. 2. Launch Trajectory of Explorer I

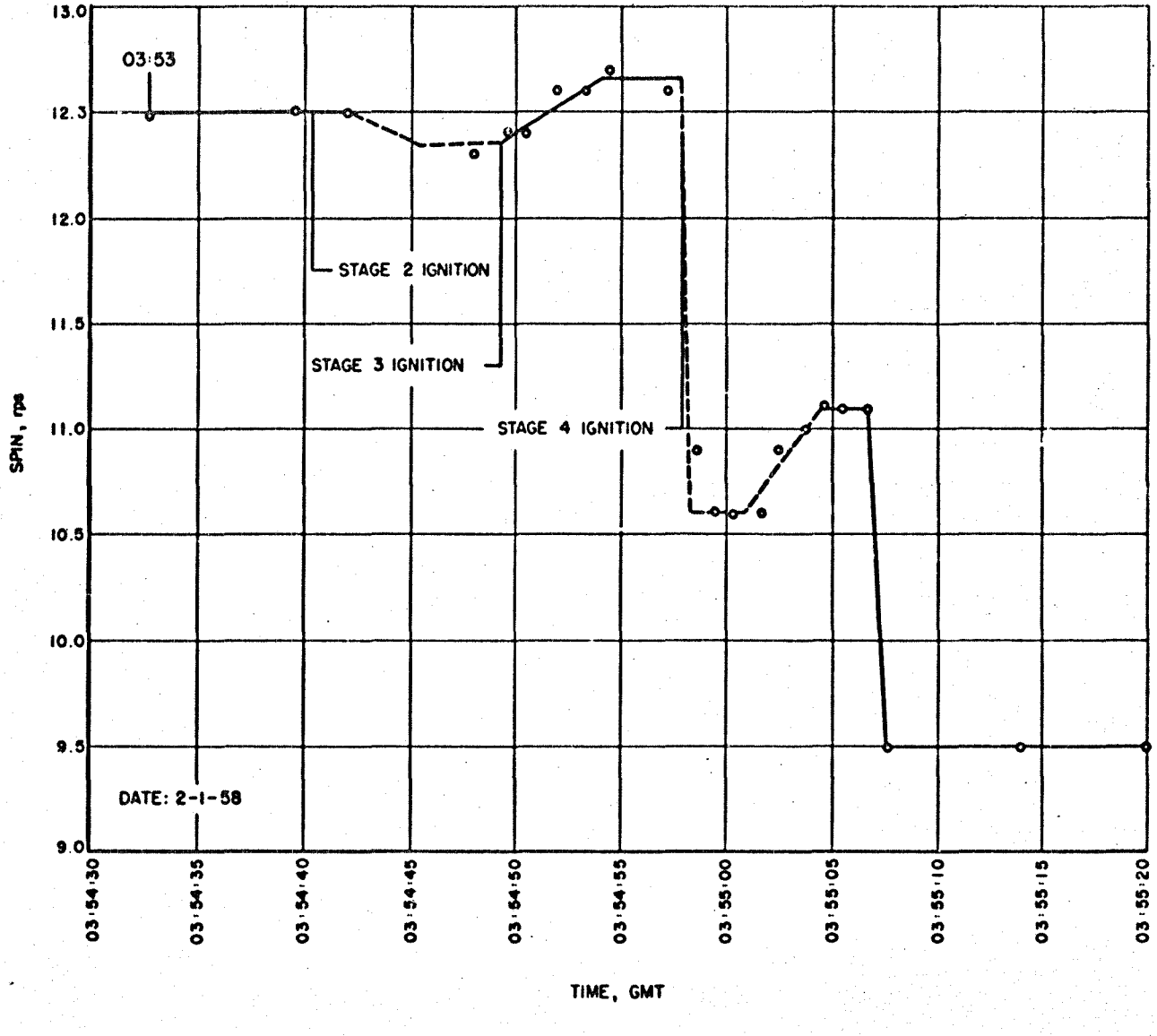

Fig. 3. Plot of Spin Rate vs Time for Explorer I During High-Speed Staging

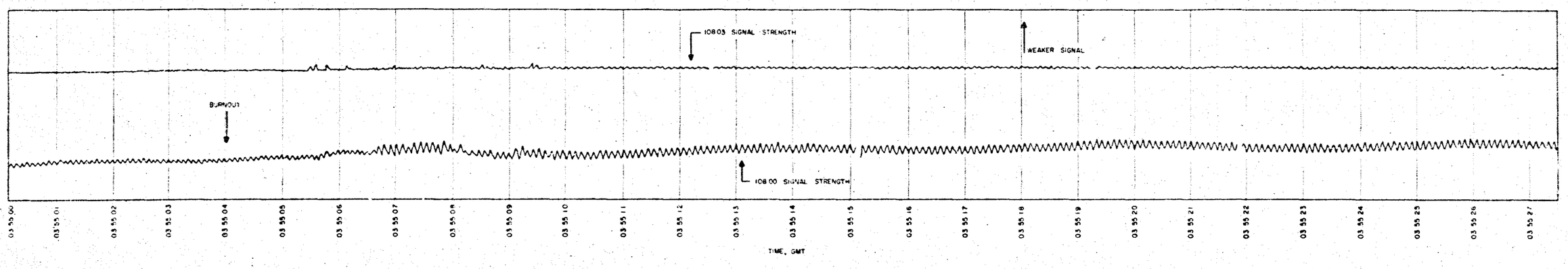

Fig. 4. Reproduction of a Portion of the Signal-Strength Record of Explorer I

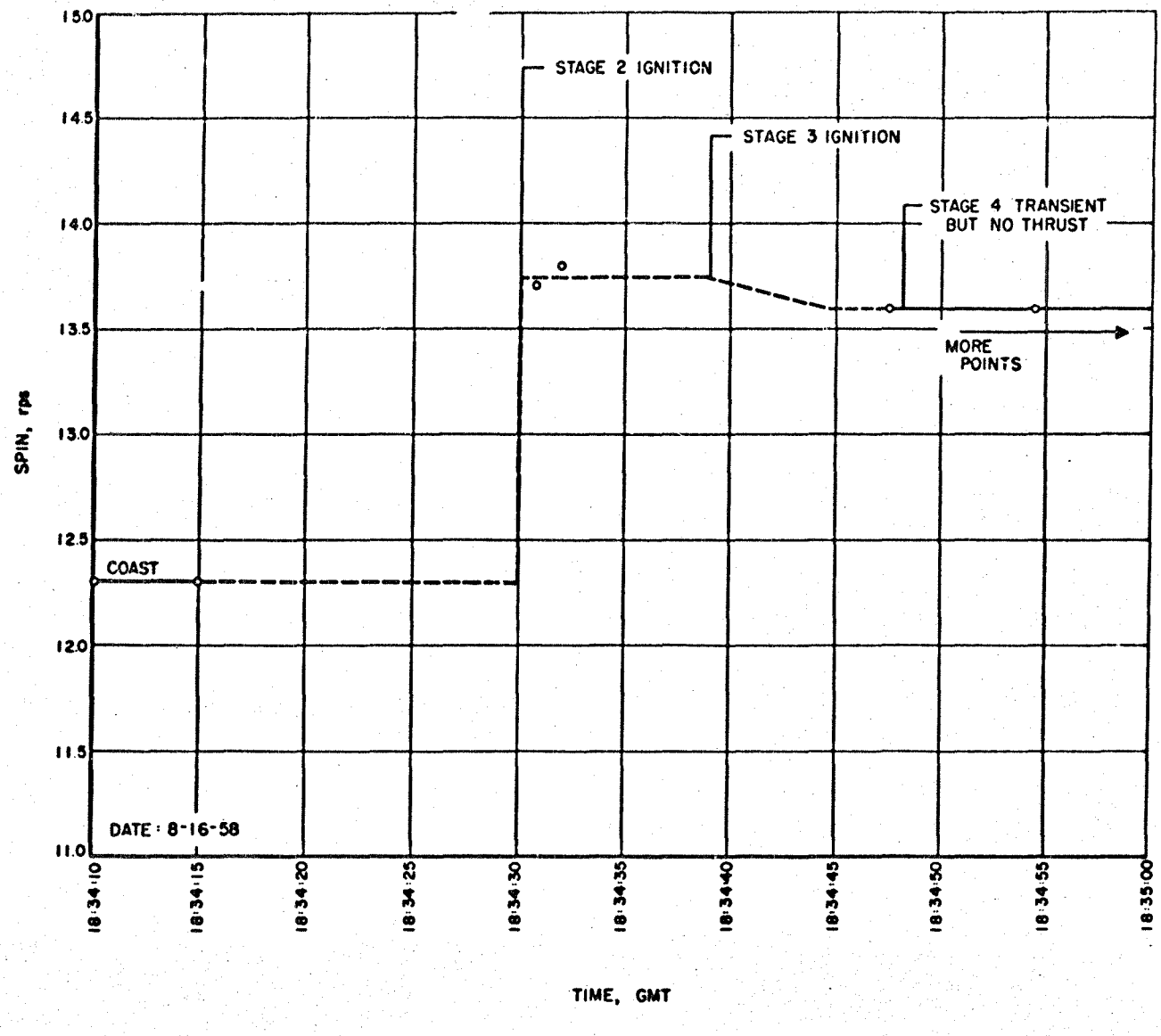

Fig. 5. Plot of Spin Rate vs Time for Explorer II During High-Speed Staging

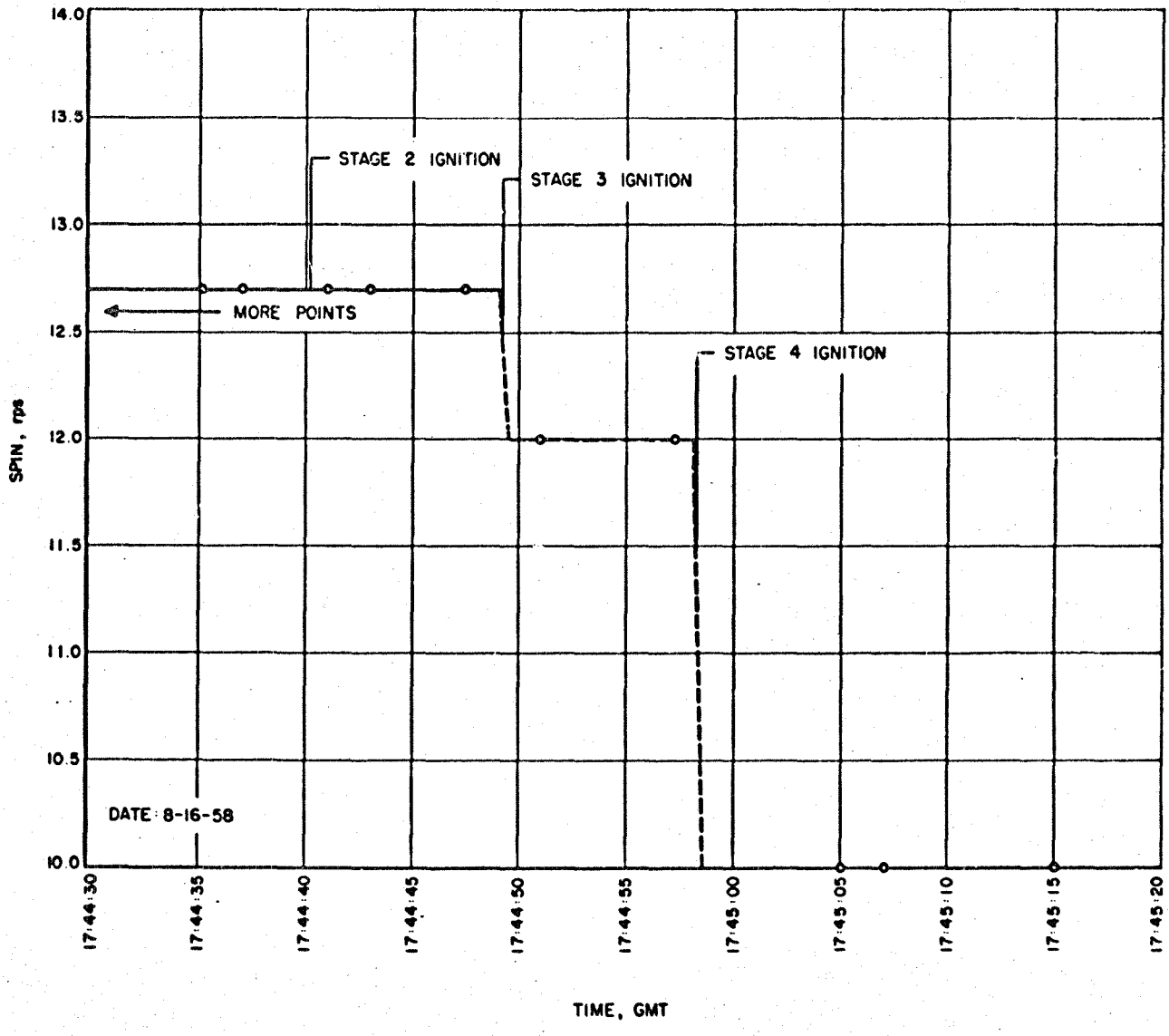

Fig. 6. Plot of Spin Rate vs Time for Explorer III During High-Speed Staging

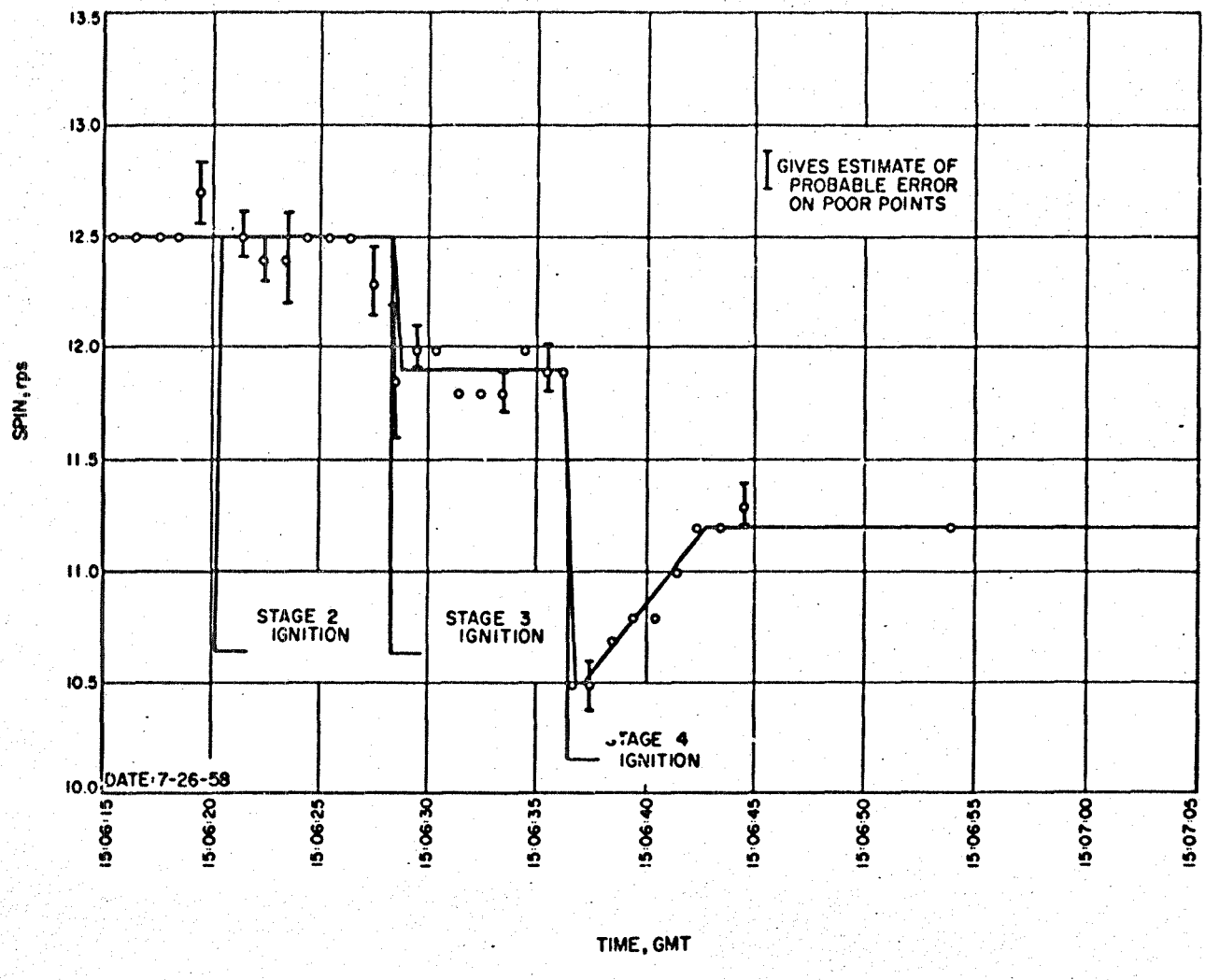

Fig. 7. Plot of Spin Rate vs Time for Explorer IV During High-Speed Staging

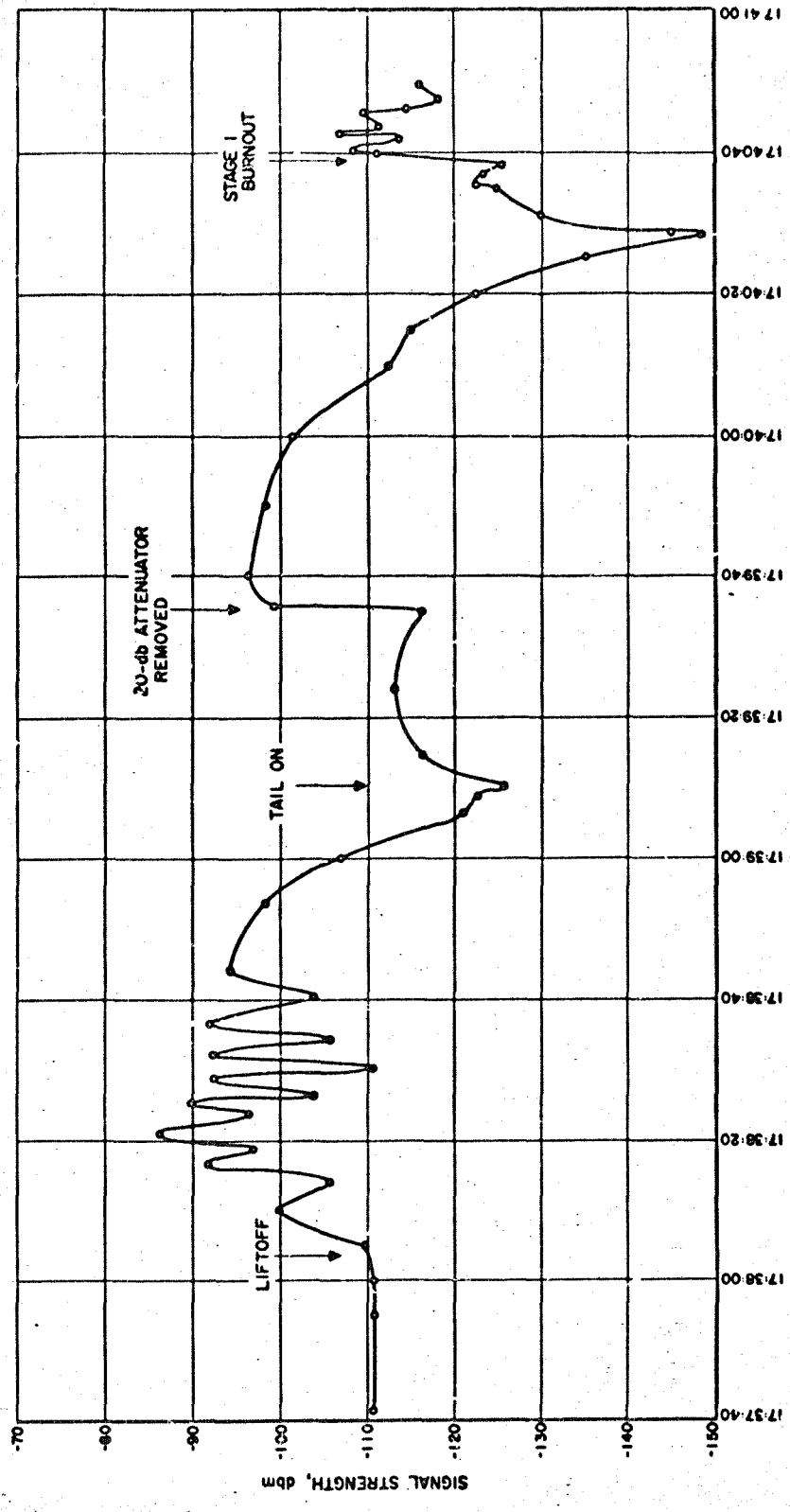

Fig. 8a. Plot of Signal Strength vs Time for Explorer III Launch

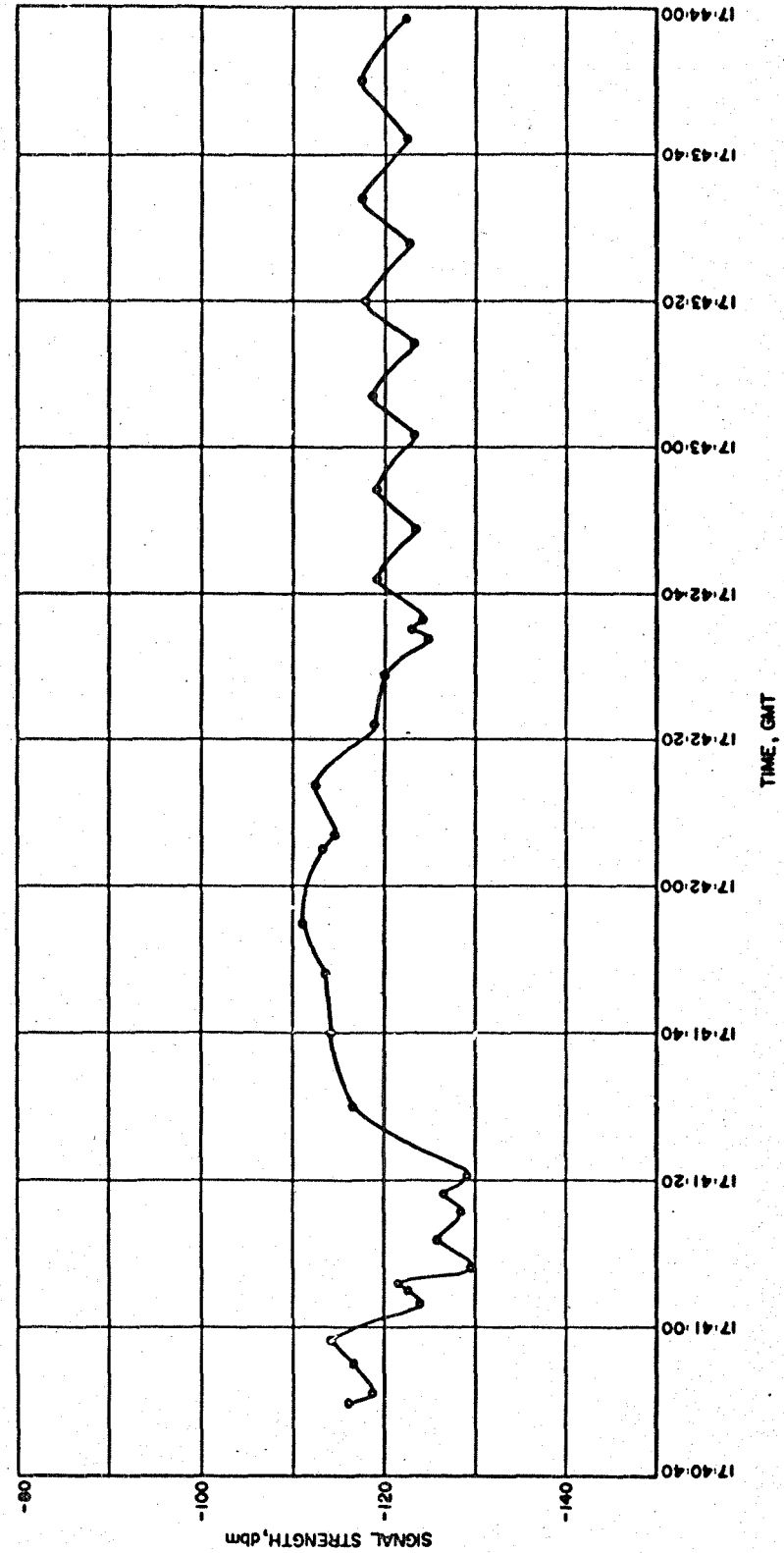

Fig. 8b. Plot of Signal Strength vs Time for Explorer III Launch

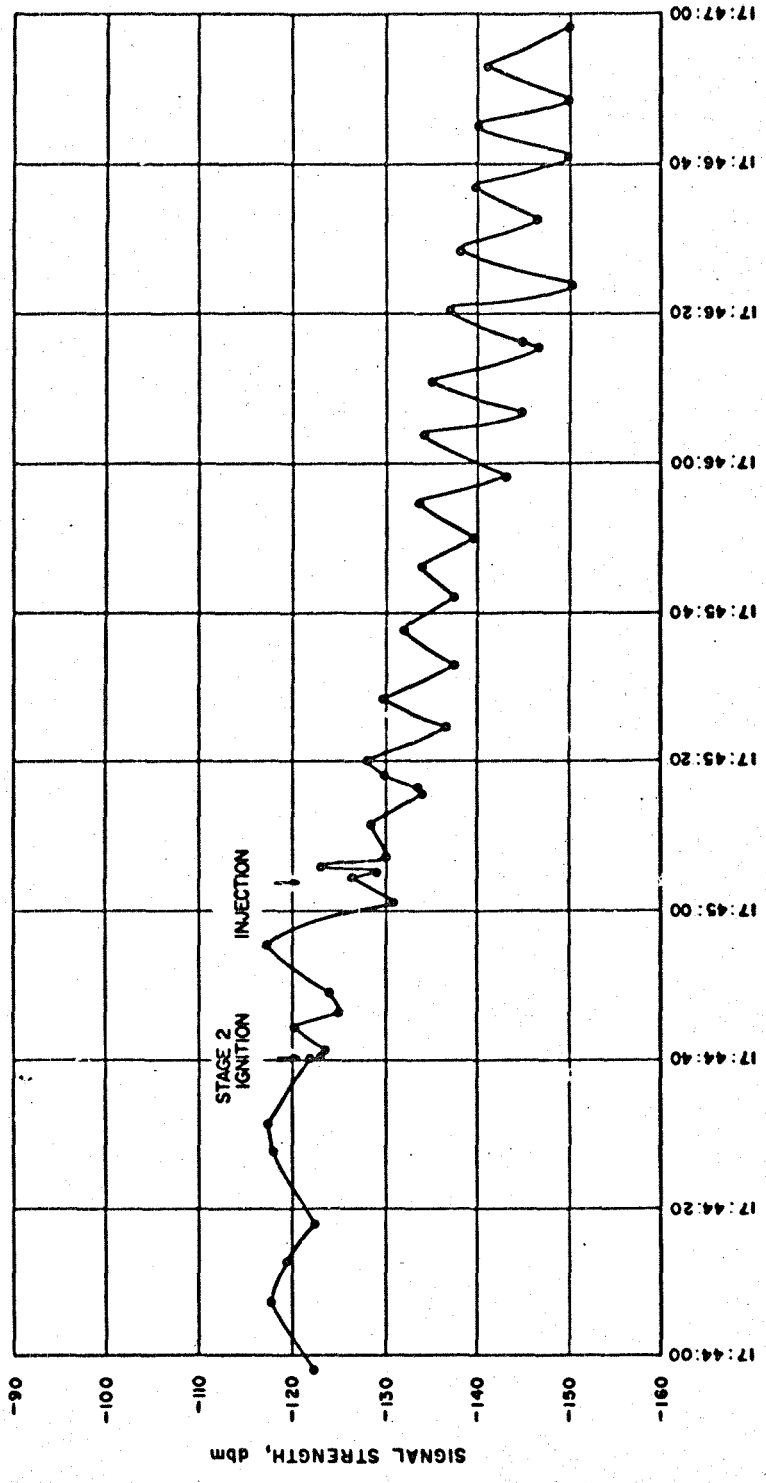

Fig. 8c. Plot of Signal Strength vs Time for Explorer III Launch

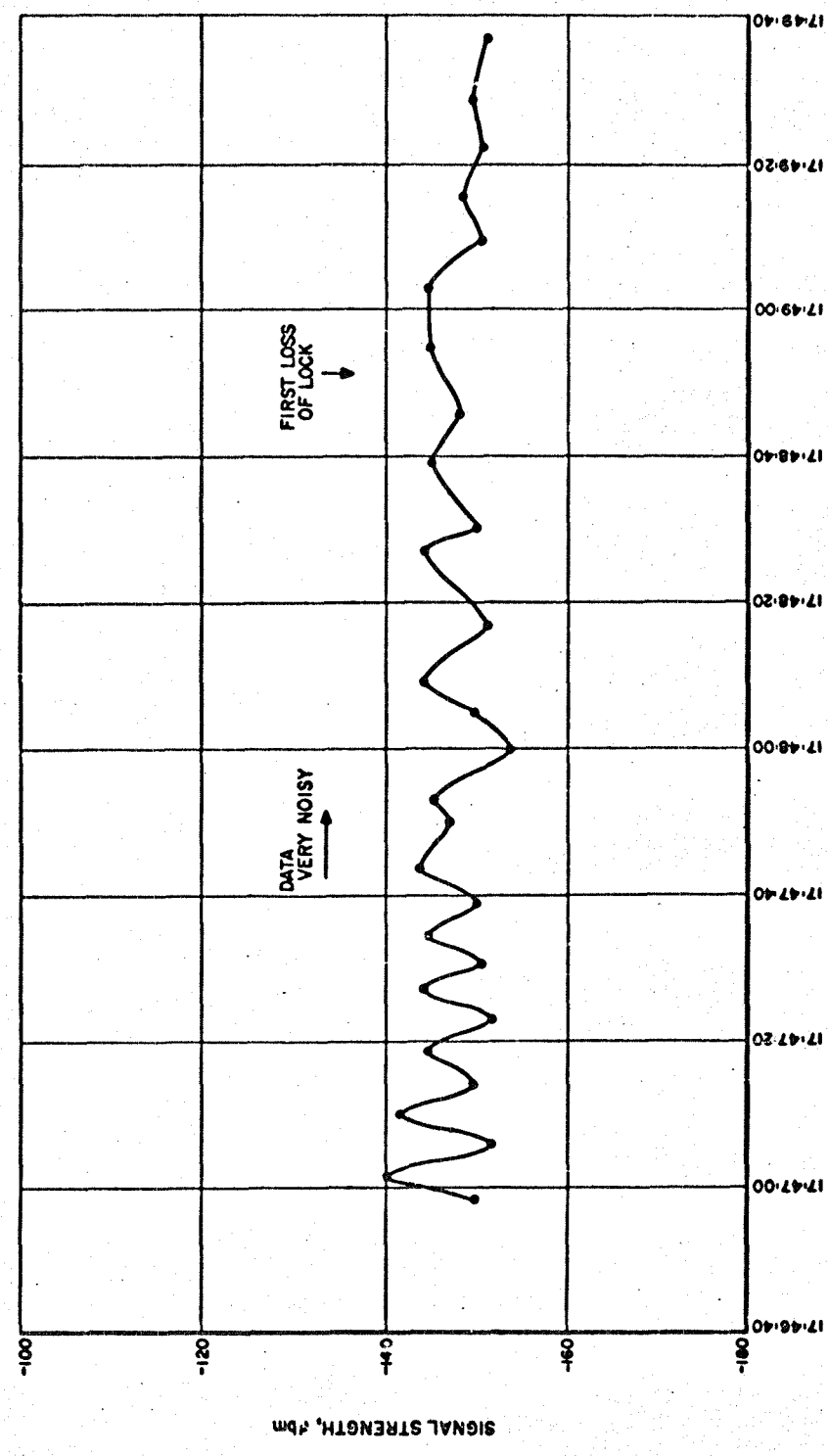

Fig. 8d. Plot of Signal Strength vs Time for Explorer III Launch

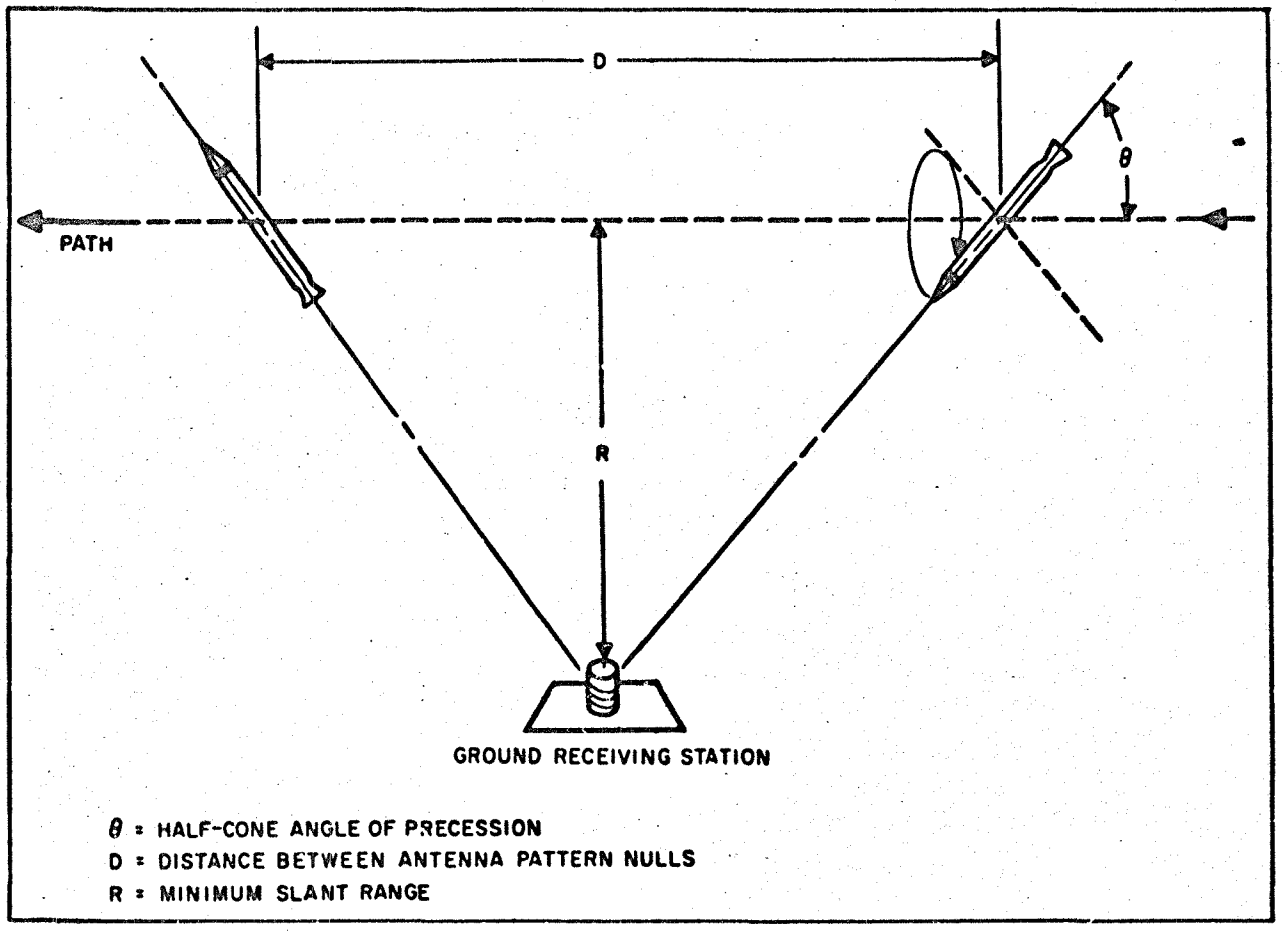

Fig. 9. Method of Obtaining Cone Angle of Precession by Direct Evaluation of Signal-Strength Records

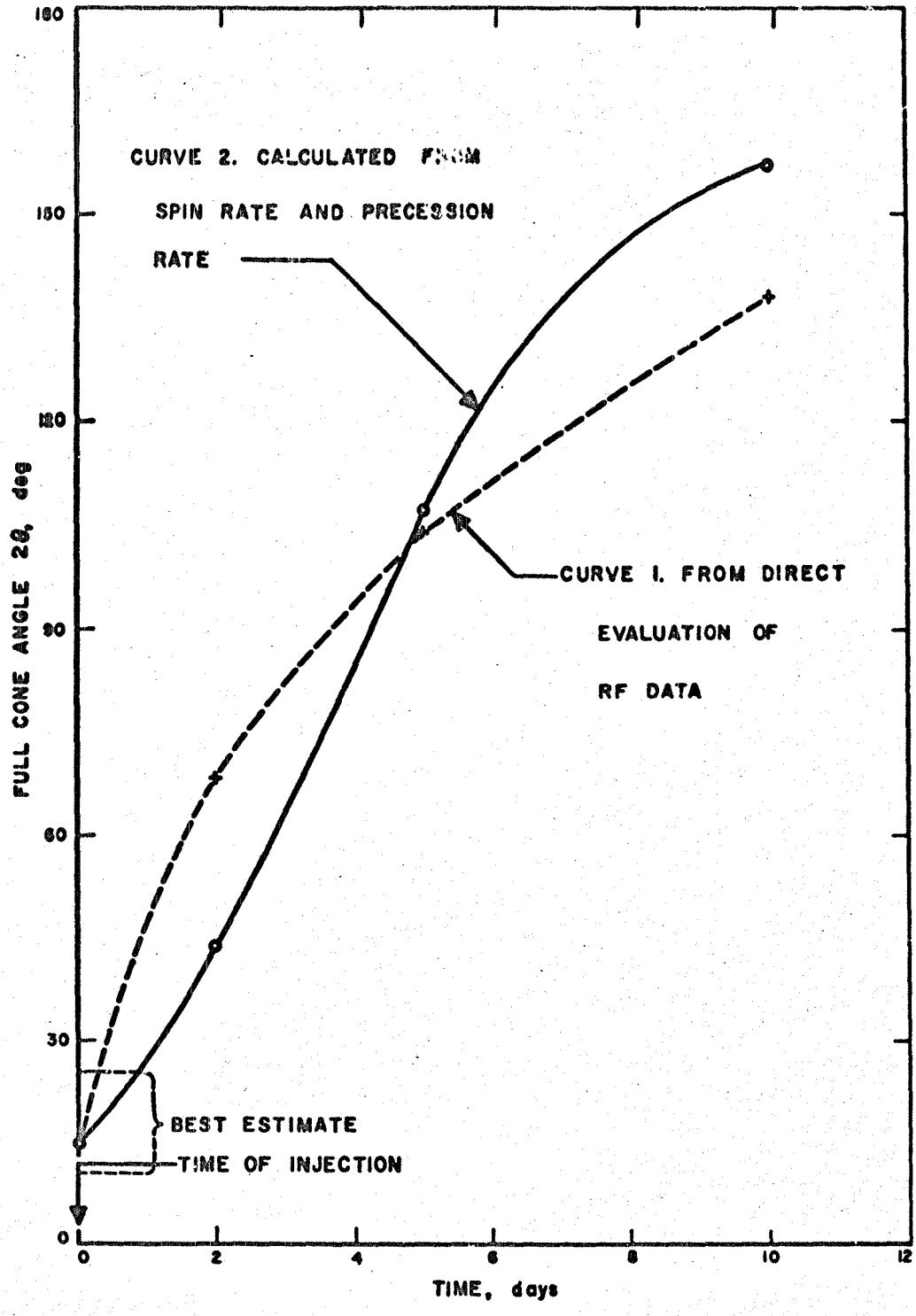

Fig. 10. Plot of Approximate Cone Angle of Precession vs Time

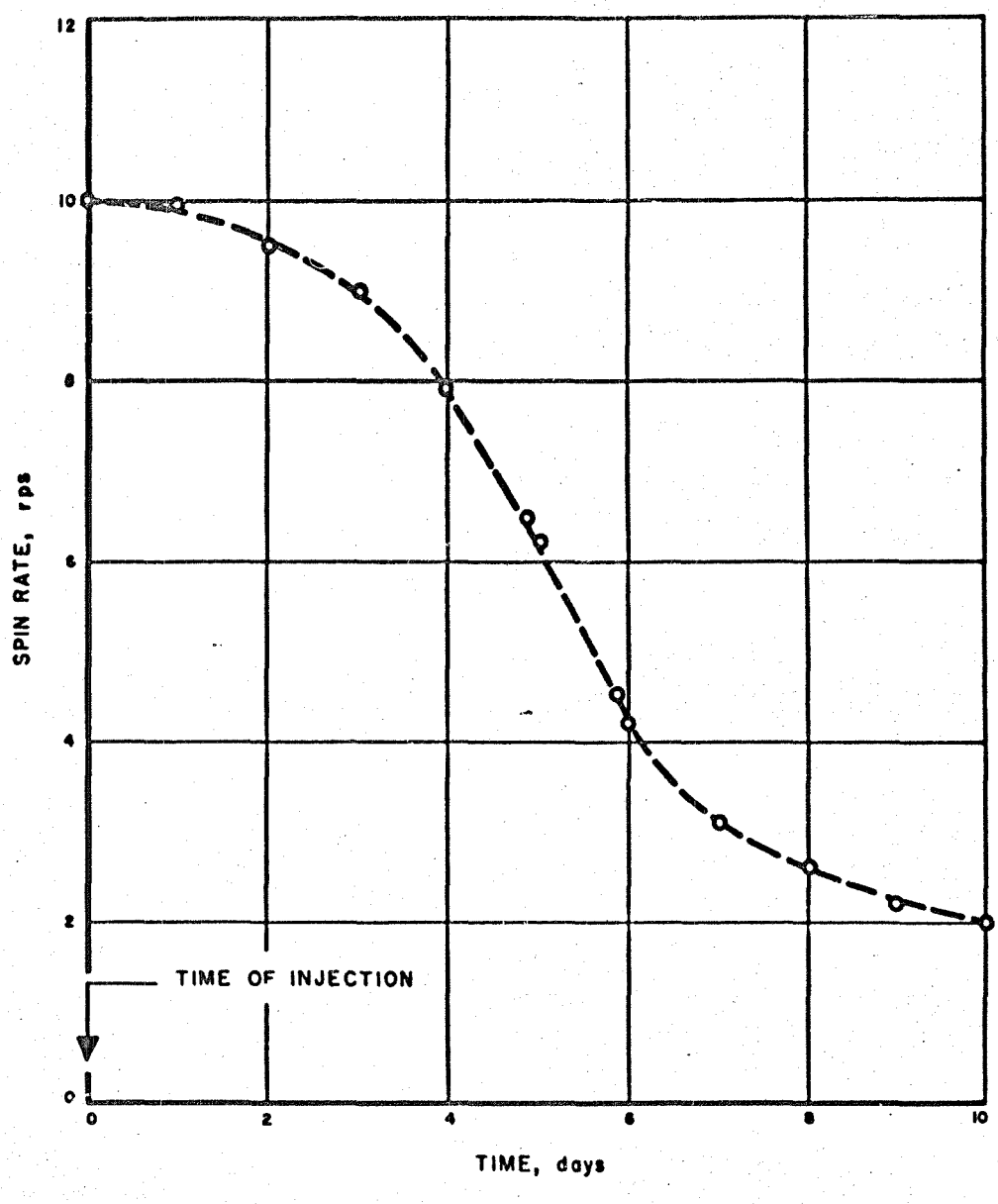

Fig. 11. Plot of Spin Rate vs Time for Explorer III After Injection

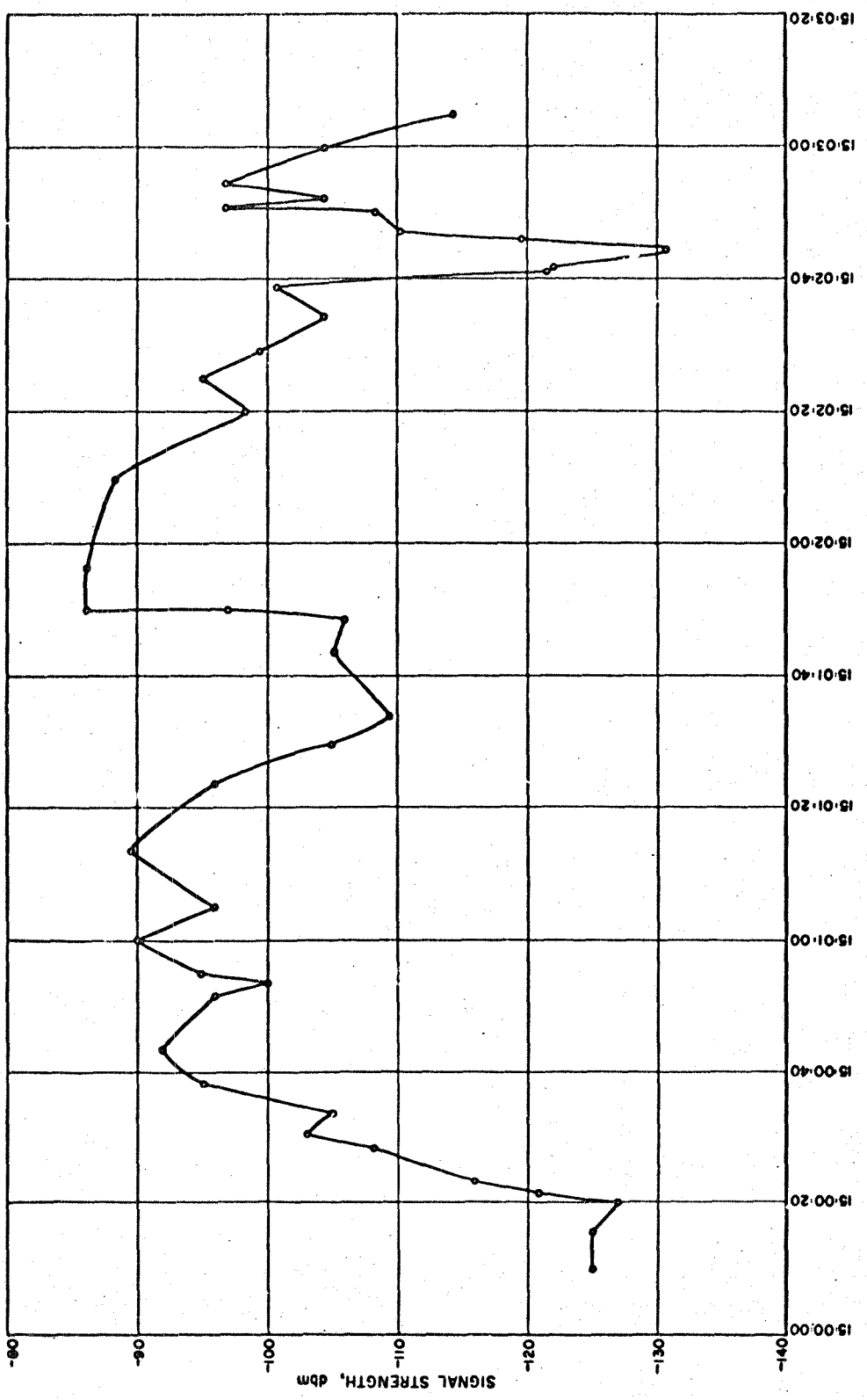

Fig. 12a. Plot of Signal Strength vs Time for Explorer IV Launch

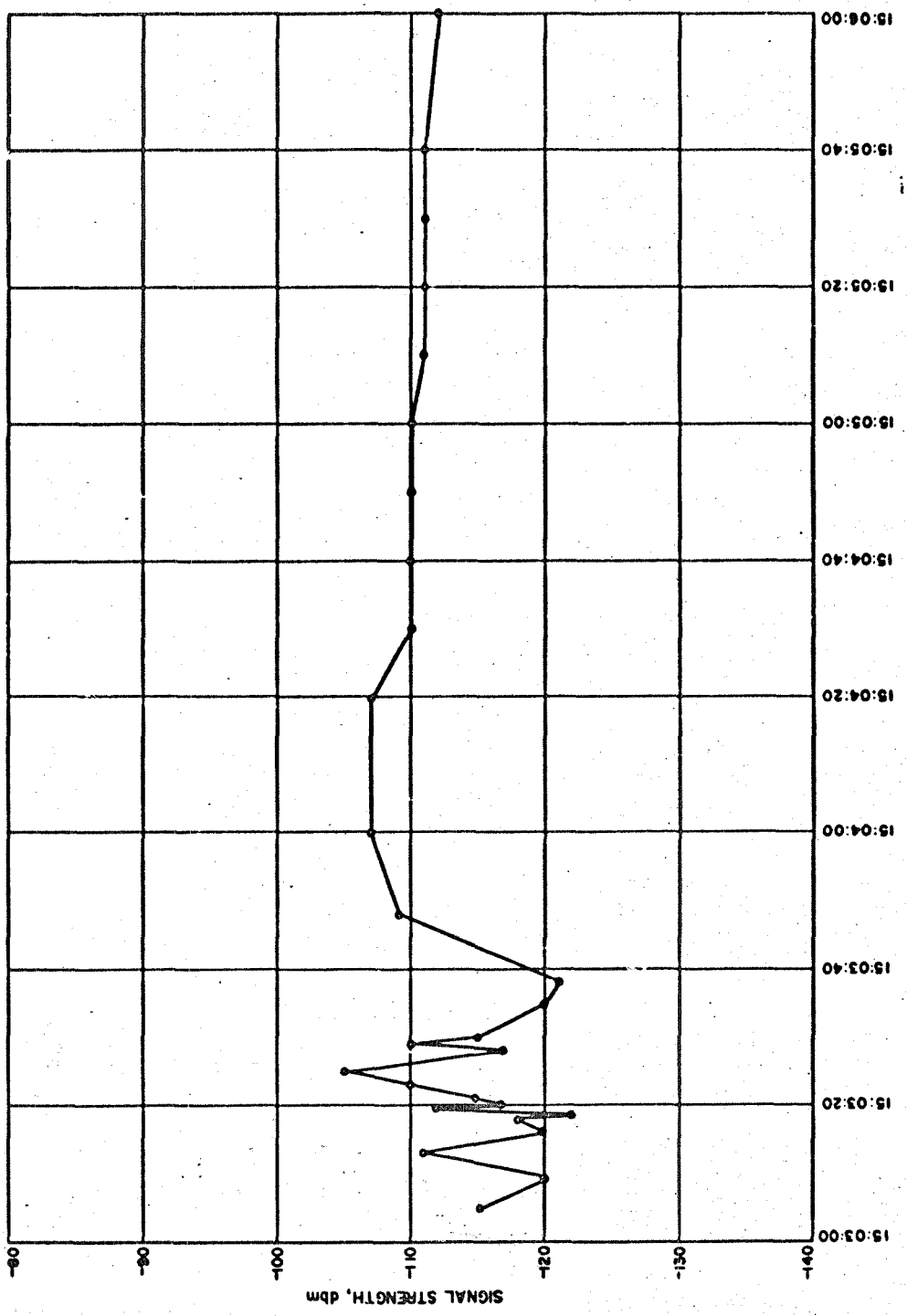

Fig. 12b. Plot of Signal Strength vs Time for Explorer IV Launch

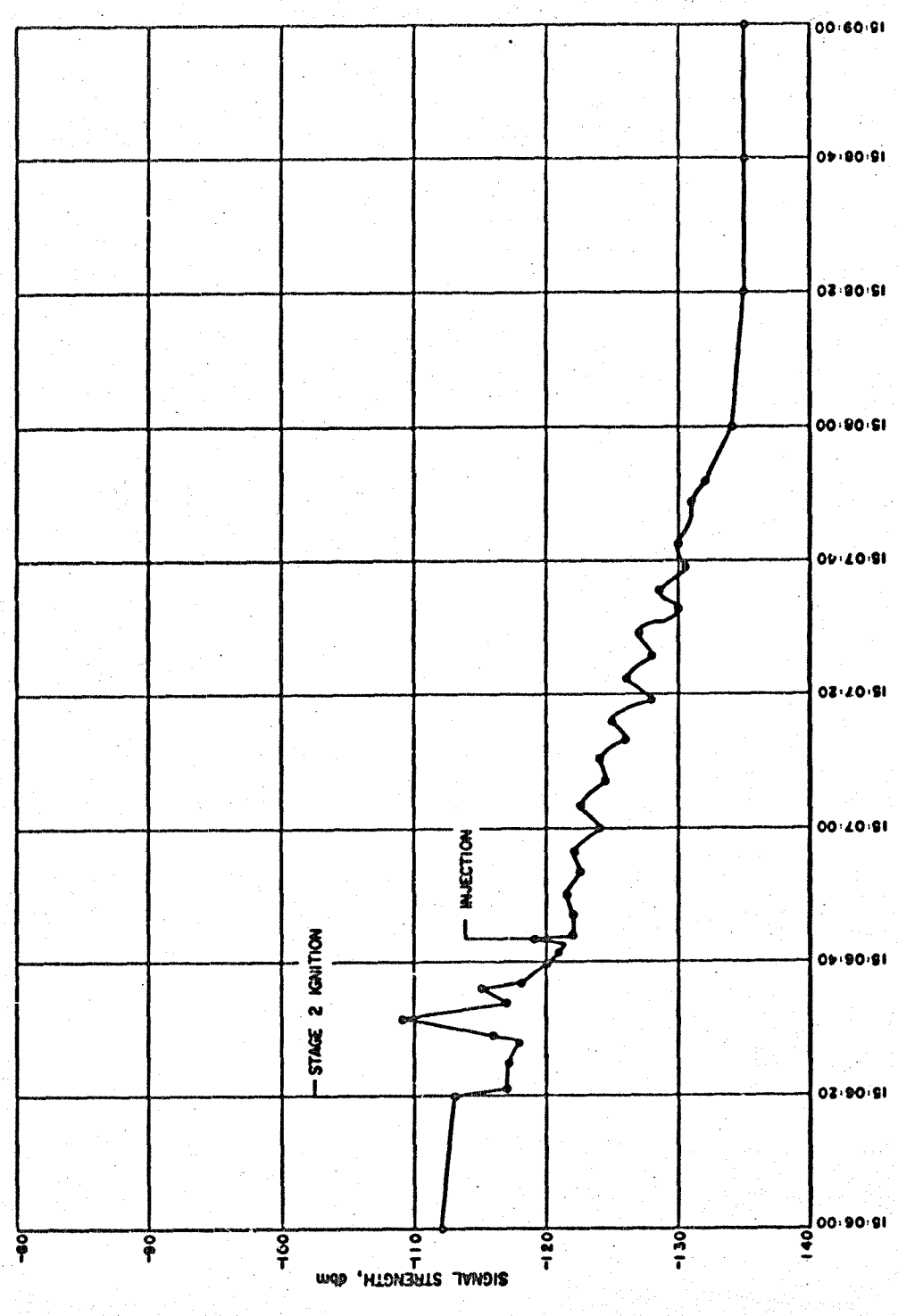

Fig. 12c. Plot of Signal Strength vs Time for Explorer IV Launch

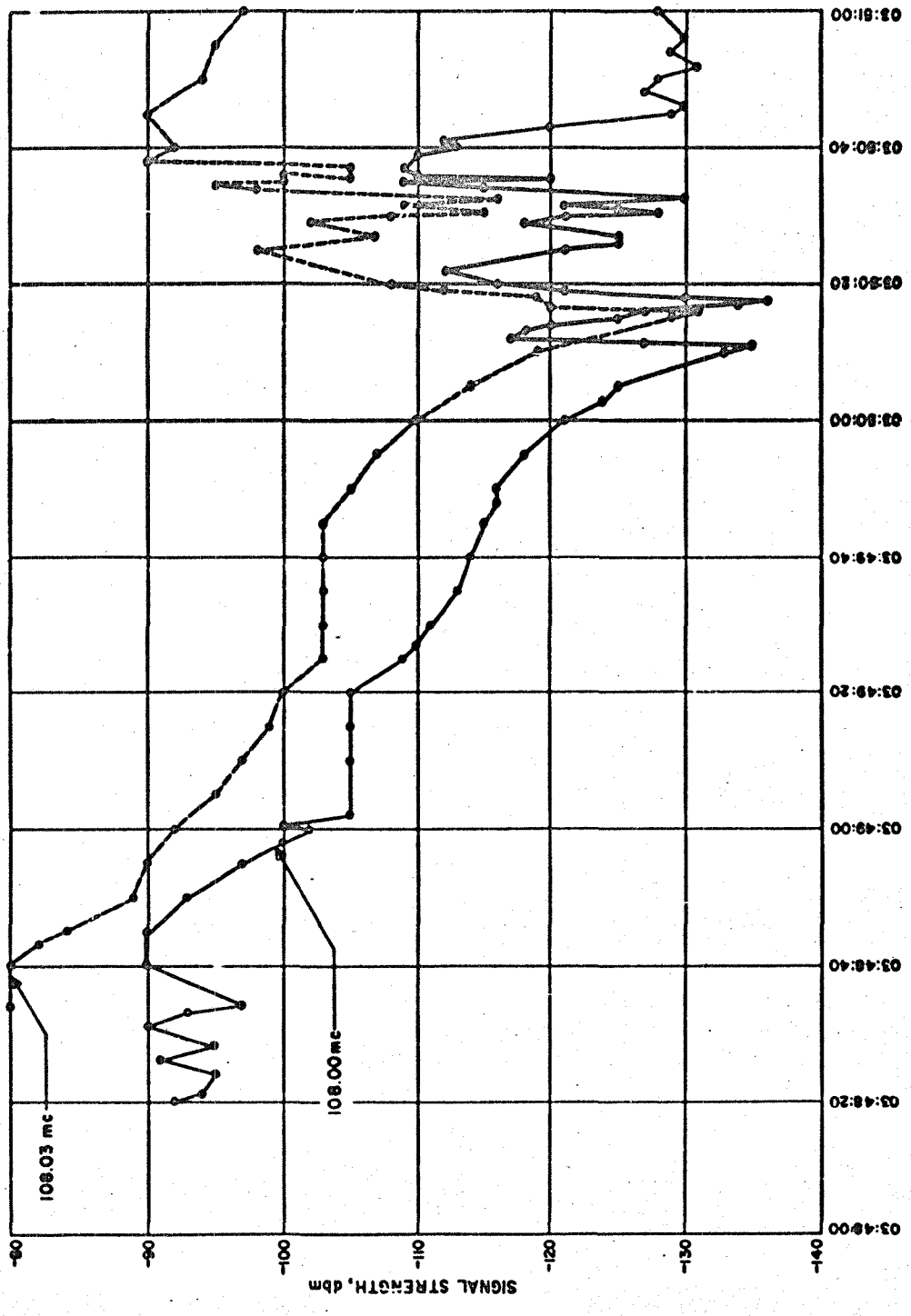

Fig. 13a. Plot of Signal Strength vs Time for Explorer I Launch

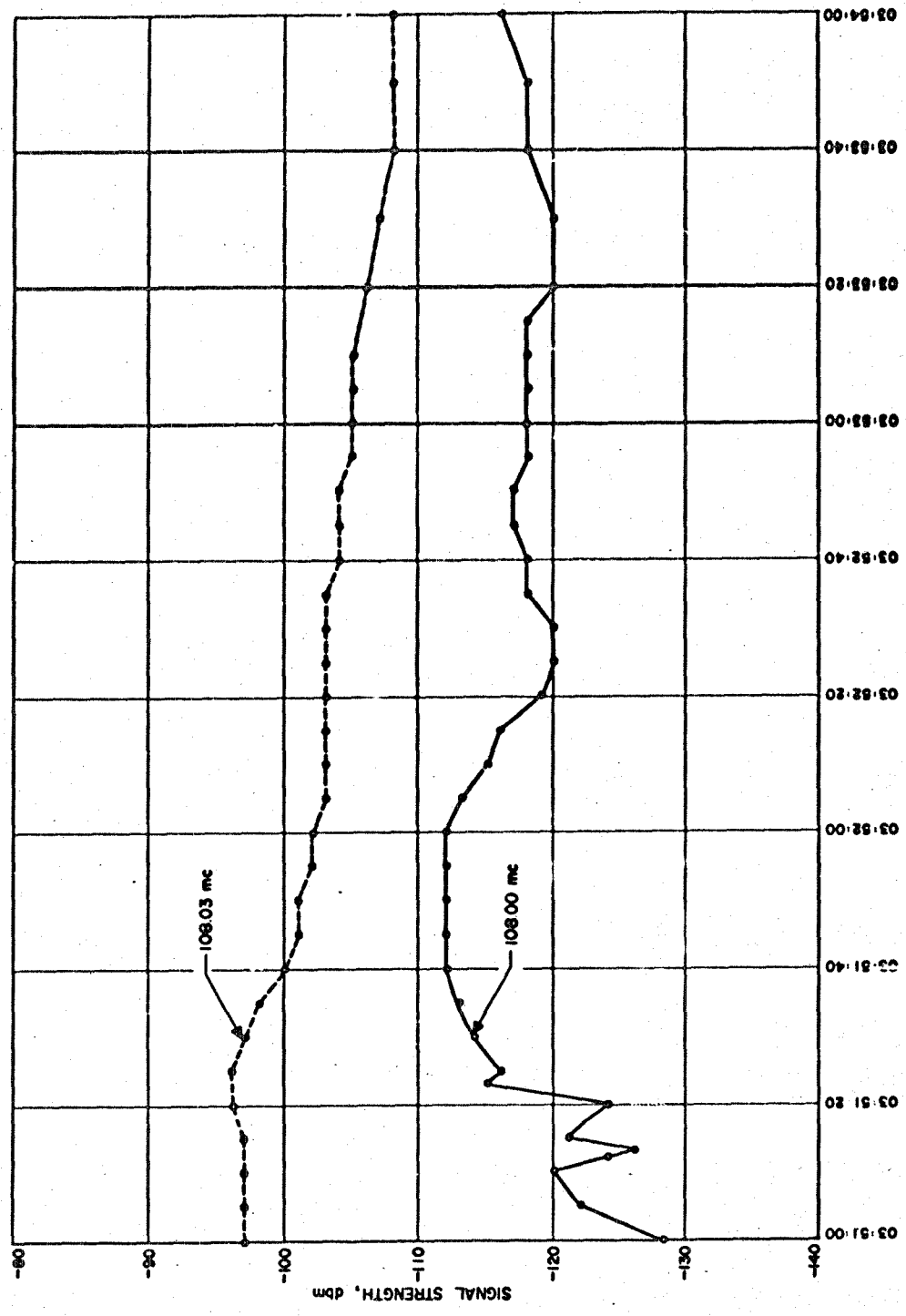

Fig. 13b. Plot of Signal Strength vs Time for Explorer I Launch

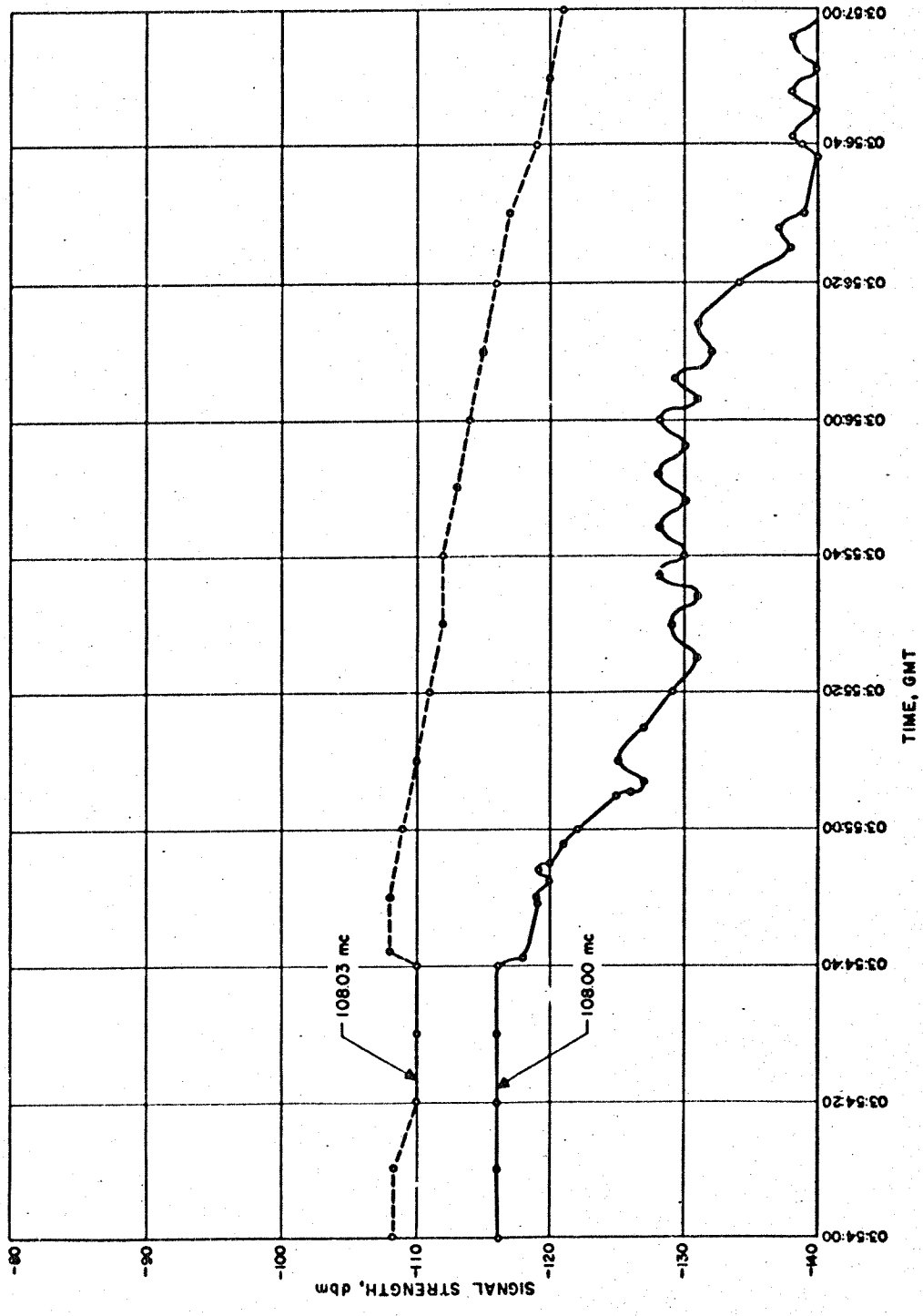

Fig. 13c. Plot of Signal Strength vs Time for Explorer I Launch

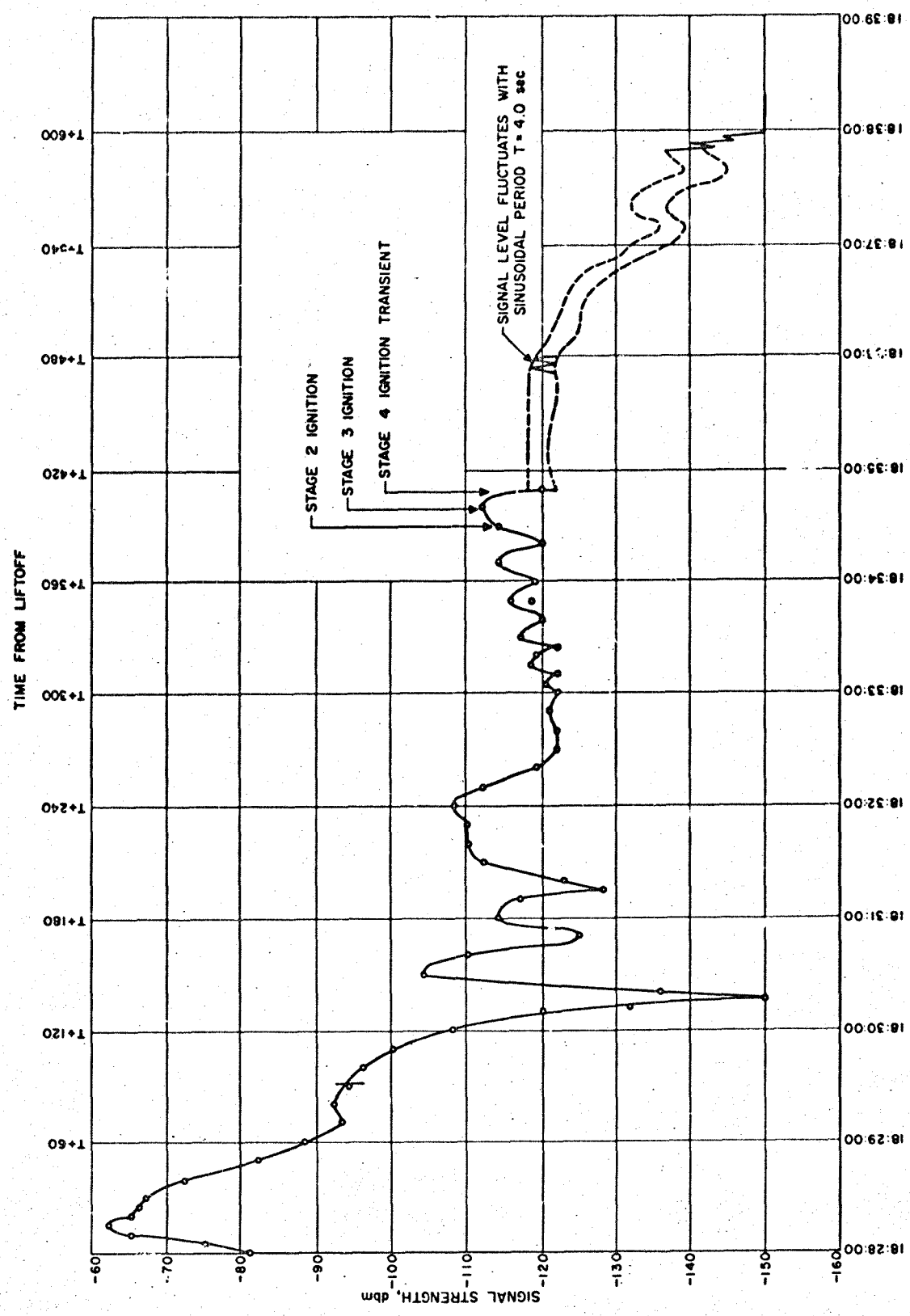

Fig. 14. Plot of Signal Strength at 108.00 mc vs Time for Explorer II

Appendix A. Explorer I and III Instrumentation

Description of Explorer I Circuitry

Explorer I was a very simple and very reliable satellite. It contained two separate transmitters, each with its own battery supply, its own telemetering oscillators, and its own antennas. The transmitters were interconnected only through RF coupling between the two antennas and through the sharing of input data by one channel of telemetering in each unit.

A block diagram of the Explorer I instrumentation is shown in Fig. A-1. The low-power transmitter was a 10-milliwatt unit at 108.00 mc with an expected lifetime of 2 to 3 months. It had a 54-mc transistor oscillator which was phase-modulated by 4 channels of RDB telemetering, channels 2 through 5. Channel 2 was a skin-temperature measurement; channel 3, a nose-cone-temperature measurement; channel 4, a micrometeorite-impact measurement; and channel 5, a cosmic-ray count.

In the type of telemetry used, the information was carried as the frequency of these audio-frequency telemetering oscillators. Thus, four separate variable audio frequencies modulated the carrier. The phase modulation was approximately 14 deg per telemetering channel. This 54-mc phase-modulated signal was then doubled and amplified in another transistor. The output of this doubler amplifier was matched to the antenna with a simple matching network. The antenna was an unsymmetrical dipole driving the nose cone against the shell of the package. A schematic diagram of the low-power transmitter is shown in Fig. A-2, and Fig. A-3 is a photograph of the unit.

The 108.03-mc beacon was a 60-milliwatt unit with a life expectancy of approximately 2 weeks. The block diagram is very similar to that of the 108.00-mc unit, the only difference being that instead of phase modulation on the oscillator itself, amplitude modulation was applied at the collector of the doubler amplifier. Incidental phase modulation was also present. Thus, the signal from the high-power transmitter could be received and the telemetering reduced with a receiver set up for either amplitude modulation or small-angle phase modulation. The antenna in this case was a turnstile antenna. The 60-milliwatt output of the transmitter was matched to this turnstile antenna with lengths of 50-ohm miniature cable. These lengths were cut so as to produce approximately 90 deg of phase rotation from each antenna to the next. Actually, the circular pattern was designed to have some ellipticity so that spin could easily be measured from the RF received signal-strength record.

The high-power-beacon telemetry was as follows. Channel 2 measured skin temperature at a point to the rear of the point measured by the low-power beacon. Channel 3 was an internal temperature measurement. On channel 4, another form of micrometeorite measurement was made. On channel 5 the cosmic-ray count was again telemetered.

The temperature measurements in a satellite have the obvious purposes of determining the shell temperature and the success with which the internal temperature has been averaged. These temperature measurements were made with various simple resistance thermometers.

The density and relative momentum of micrometeorites are of importance from both a scientific and an engineering standpoint. On the 60-milliwatt unit a micrometeorite with sufficient momentum impacting upon the skin of the satellite near a microphone in spring contact with the skin actuated a scaler. The output of the scaler controlled the frequency of the channel 4 subcarrier, causing it to change from one to the other of two possible frequencies for each impact. Thus a change from high to low or from low to high frequency indicated an impact with a micrometeorite having a momentum above a calibrated threshold. The impact momentum necessary to trigger the scaler was about 10^{-2} g-cm/sec with variations depending on how close to the microphone the impact occurred. This experiment was suggested by Dr. M. Dubin and Dr. E. Manring of the Air Force Cambridge Research Center (AFCRC).

Channel 4 on the 10-milliwatt unit measured micrometeorite erosion by a technique different from that used on the high-power transmitter. A wire-grid device was located on the outside skin of the satellite so that particles of sufficient size and relative velocity would cause a cratering effect capable of severing a wire. The gauge was composed of 12 grids in parallel. If any grids had been broken, the resistance-controlled oscillator would have changed frequency in discrete steps. This wire-grid gauge, also suggested by Drs. Dubin and Manring, was supplied by AFCRC.

Cosmic-ray-count information, detected by a Geiger-Mueller tube, caused the final stage of a scaler to change state every 16 counts. The voltage output of this scaler put the subcarrier oscillator at

either one of two frequencies for each 16 counts, thus measuring the number of particles impinging on the Geiger-Mueller tube. This experiment was suggested by Dr. James Van Allen of the State University of Iowa (SUI). The experiment was modified by the Jet Propulsion Laboratory and by George Ludwig of SUI to fit the requirements of the Explorer.

Figure A-4 is a cutaway drawing showing the arrangement of the instrumentation in both Explorers I and III. Figure A-5 is a photograph of the Explorer I payload with the outer shell removed.

The performance of the Explorer I experiment was excellent; Table A-1 summarizes the characteristics. The effective radiated powers were approximately 10 and 60 milliwatts, their short-term frequency stability was of the order of 1 part in 10^7, the telemetry was good, and their life in orbit was approximately that desired. The high-power unit stopped a day or so before its predicted end of life, but after approximately 2 weeks it fortunately resumed transmitting for several days to add significant data. The low-power transmitter operated almost 4 months and telemetered data in a satisfactory way for almost 3 months.

Description of Explorer III Circuitry

Explorer III also contained two separate and different telemetering systems. Figure A-4, a cutaway view, identifies the major parts. A block diagram of Explorer III is presented in Fig. A-6. The 108.00-mc transmitter radiated approximately 10 milliwatts of RF continuously. It was almost identical to the unit flown in Explorer I; it had a 54-mc oscillator which was phase-deviated by four channels of telemetering.

These channels measured the skin temperature, the internal temperature, the number of micrometeorites of sufficient size to break small erosion gauge wires, and the cosmic-ray count. The phase-modulated output of the 54-mc oscillator was doubled and amplified in a final transistor stage and then matched to an unsymmetrical dipole antenna made up of the nose cone and the shell of the package. This transmitter operated continuously and was used for position determination of the device as well as for telemetering.

The other transmitter was at 108.03-mc and radiated approximately 60 milliwatts. This unit did not transmit continuously but was interrogated from the ground and transmitted only for a few seconds on each pass. This unit received a signal from the ground on an antenna made up of the last-stage motor case and the shell containing the satellite instrumentation. This signal passed through a filter into a receiver which decided whether or not there was a valid interrogation. When the decision was made that there had been a valid interrogation, the transmitter was keyed on, and the tape recorder read out all of the cosmic-ray information stored during a complete circuit of the earth. The incident radiation produced counts in a Geiger-Mueller tube, and these were recorded on a very slow-moving tape recorder in a modified State University of Iowa experiment. After interrogation, this tape recorder played back very rapidly and produced amplitude modulation of a transmitter very similar to the one described as the low-power 108.00-mc beacon; the main difference was that the 54-mc oscillator was 15-kc higher,

producing 108.03-mc output when doubled. The amplitude modulation was somewhat different from that used in Explorer I in that base modulation was used, but the end result was very similar. The output of this transmitter was matched onto the same antenna as the receiving interrogation antenna; the frequencies were sufficiently different to allow this duplexing.

A brief performance comparison of the two transmitters might be in order at this point. The high-power interrogated transmitter had an output of approximately 60-milliwatt average power. Its modulation was essentially square wave and very close to 100 % modulation. It carried only the one channel of telemetering; in approximately 7 sec it relayed back 2 hr of cosmic-ray data recorded at 1-sec intervals. The stability of the unit is not of particular significance for this operation, but during the interrogation the transmitter was stable within approximately 100 cyc. The expected life of all the units that made up the high-power transmitter was approximately 2 months. The low-power transmitter had a continuous output of approximately 10 milliwatts. It had phase modulation of approximately 14 deg on each of the four channels of telemetry. It is to be noted that channel 5 on the low-power transmitter also sent back the cosmic-ray count. This transmission was continuous, and thus, although the unit lacked the feature of storage, it did have somewhat wider range than the tape unit. The short-term frequency stability of the low-power beacon was of the order of 1 part 10^7. The expected life of this unit was also 2 months.

The modified SUI experiment is shown in block-diagram form in Fig. A-7. The counts produced by incident cosmic rays are scaled

by a factor of 32. One of the two outputs from this scale of 32 goes to channel 5 of the low-power beacon. The second output of the scaler goes to a scale of 4 and then to one input of a blanking circuit. The other input of the blanking circuit comes from a 512-cps tuning fork scaled down to produce a 1-sec pulse. Whenever a count of 128 has been reached in the Geiger-Mueller tube, a pulse is not recorded. At all other times 1-sec pulses are recorded on the tape recorder, which moves forward 0.005 in./sec. When the system is interrogated, the tape rewinds quite rapidly onto the original spool and passes by the playback head. These square-wave pulses, passing the head at about a 1-kc rate, modulate the high-power transmitter. A pulse is missing every time the Geiger-Mueller tube has counted 128 pulses. The total playback takes approximately 7 sec. The transmitter is turned off, and the unit then recycles and begins stepping forward at 0.005 in./sec, until the next interrogation.

Typical Explorer Data Calibration

The calibration curve of the channel 2 skin-temperature measurement of the low-power transmitter is shown in Fig. A-8. These calibrations, made at 0, 25, and 50°C, clearly show the temperature coefficient of the oscillator. If no information on the oscillator temperature were available, considerable error in measurement of the internal and external temperatures would occur. The internal temperature measurement, although not directly measuring the temperature of the subcarrier oscillators, provided a good estimate of the oscillator temperature and determined which curve to use in reducing the data.

An accurate measurement of the subcarrier oscillator temperature was obtained by utilizing the temperature coefficient of the cosmic-ray-count circuitry. Figure A-9 shows that the frequency of each of the two possible states is strongly temperature dependent. This temperature coefficient does not affect the accuracy of the cosmic-ray-count information, but it does provide a rather precise measurement of the oscillator temperature. During data processing the frequency of each state was observed, yielding two measurements which could be compared and averaged for greater accuracy.

Ground Receiving Stations

The 108.03-mc amplitude-modulated transmission was primarily provided for Minitrack station reception. The Minitrack system has been reported upon in considerable detail in the literature and will not be discussed here. The 108.00-mc phase-modulated transmission was designed for reception by the Microlock receiving stations and for the Minitrack interferometer. Both types of stations were located at a number of points around the world within the area covered by the trajectory and recorded doppler, interferometer, and telemetering data.

Some of the performance characteristics of the Microlock system will be discussed briefly. A simplified block diagram, deleting the interferometer and doppler readout, is shown in Fig. A-10. The receiver is basically a double superheterodyne with a first IF frequency of 5 mc and a second IF of 0.455 mc. The 103-mc voltage-controlled oscillator (VCO) is phase-locked exactly 5 mc from the

108-mc incoming signal. Crystal oscillators at 5.455 mc and 0.455 mc are used as reference signals in the IF channels. The VCO is swept in frequency with an external voltage until lock, or acquisition, is obtained.

The phase detector produces a dc output voltage which is proportional to the cosine of the phase difference between the incoming signal and a reference oscillator. This output is passed through a low-pass filter which effectively removes high-frequency noise from the VCO control voltage so that the VCO output is very clean and is a good measure of the signal frequency.

In the second loop the signal is shifted in phase by 90 deg so that it is in phase with the 0.455-mc reference signal. The phase detector thus produces a dc voltage proportional to the signal amplitude (coherent signal strength).

It can be noted that the telemetering signal data do not pass through the 10-cps filter, but are recorded on magnetic tape at a point just before the low-pass loop filter. The telemetry is limited, however, by the 3-kc band pass of the IF amplifier.

As in a conventional FM-FM system, the subcarriers are separated by band-pass filters and demodulated through discriminators in order to obtain the data. A phase-locked-loop discriminator in which the threshold is proportional to the loop bandwidth is used for this reduction; it is shown in block diagram form in Fig. A-11.

The incoming subcarrier frequency, plus noise, is multiplied by a locally generated estimate of the subcarrier frequency, shifted in phase by 90 deg. An error signal proportional to the phase error between these two signals forces the VCO frequency to remain in lock

with the incoming frequency. Filtering of this error voltage need only accommodate the rate of change of the subcarrier frequency; therefore, the bandwidth can be much less than that of the more conventional discriminator. For example, on band 2, the loop bandwidth for 8-cps data need be only about 8 cps, rather than the usual predetection band-pass filter bandwidth of 84 cps. If a lower-bandwidth loop filter is employed, threshold improvement is greater, but the VCO may not automatically lock on to the incoming frequency, in which event manual acquisition techniques may have to be employed.

A section of reduced data is shown in Fig. A-12. The wide trace indicates lack of lock; the line indicates valid lock and therefore data.

In Explorer III the 108.03 transmission was interrogated at its point of closest approach. The reply was thus of sufficient signal strength so that a data bandwidth of about 1000 cps could be recorded and reduced by direct analysis of the recording for missing pulses.

Table A-1. Performance Characteristics of Explorer I

Characteristic	Low-Power Transmitter	High-Power Transmitter
Transmitter power	10 mw	60 mw
Transmitter frequency	108.00 mc	108.03 mc
Antenna type	dipole	turnstile
Maximum effective antenna gain	-2 db	+1 db
Maximum effective radiated power	+8 dbm	+18 dbm
Radiation polarization	linear	circular
Type of modulation	phase	amplitude
Amount of modulation, total of 4 subcarriers	0.7 radian rms	50%
Subcarrier frequencies, standard FM/FM channels	2, 3, 4, 5	2, 3, 4, 5
Measurement by channel assignment		
Channel 2(560 cps)	skin temperature, forward	skin temperature, rear
Channel 3(730 cps)	nose-cone temperature	internal temperature
Channel 4(960 cps)	wire-grid micrometeorite detection	microphone-micrometeorite detection
Channel 5(1300 cps)	cosmic-ray count	cosmic-ray count
Expected life	2 months	2 weeks

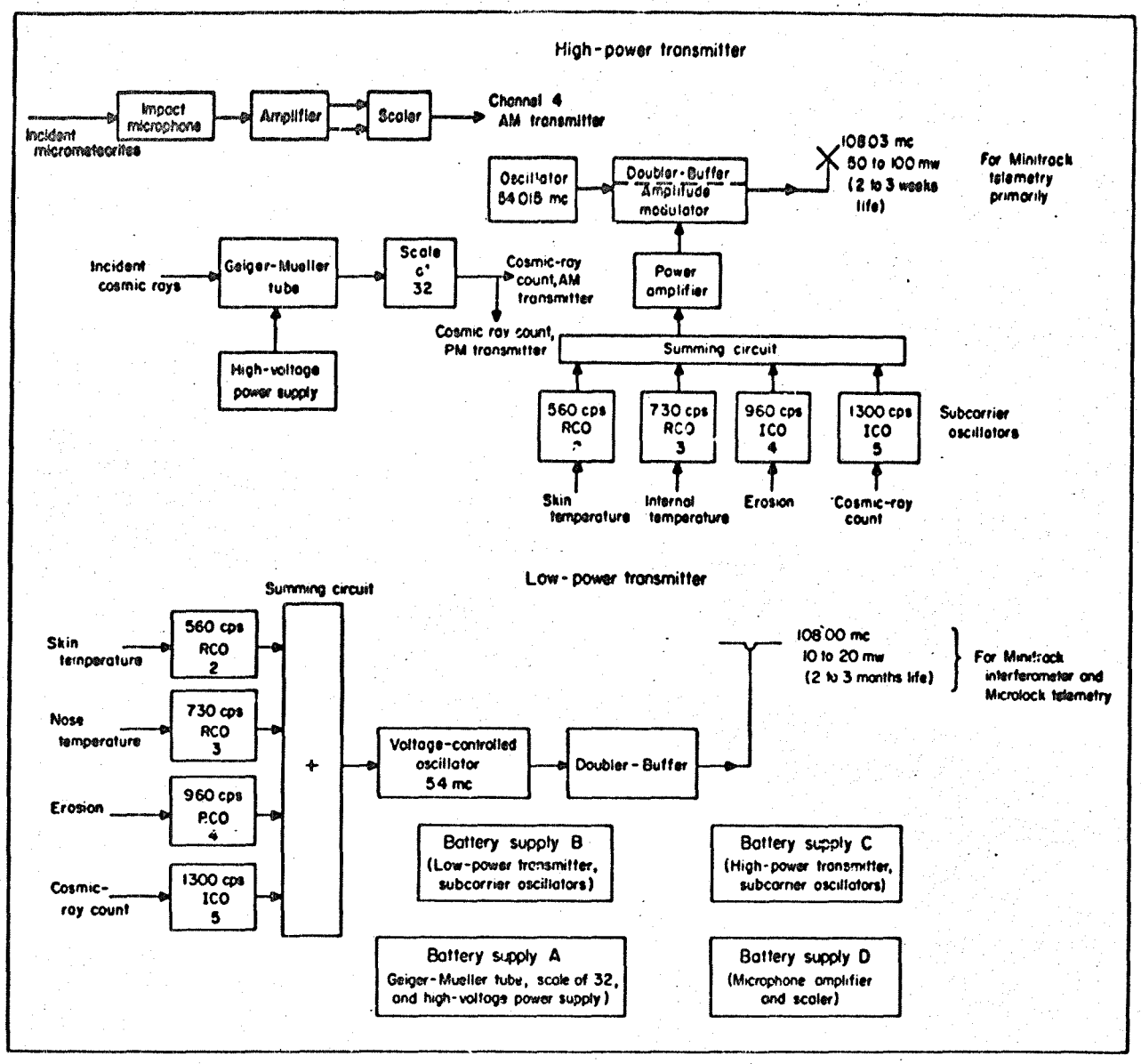

Fig. A-1. Block Diagram of Explorer I

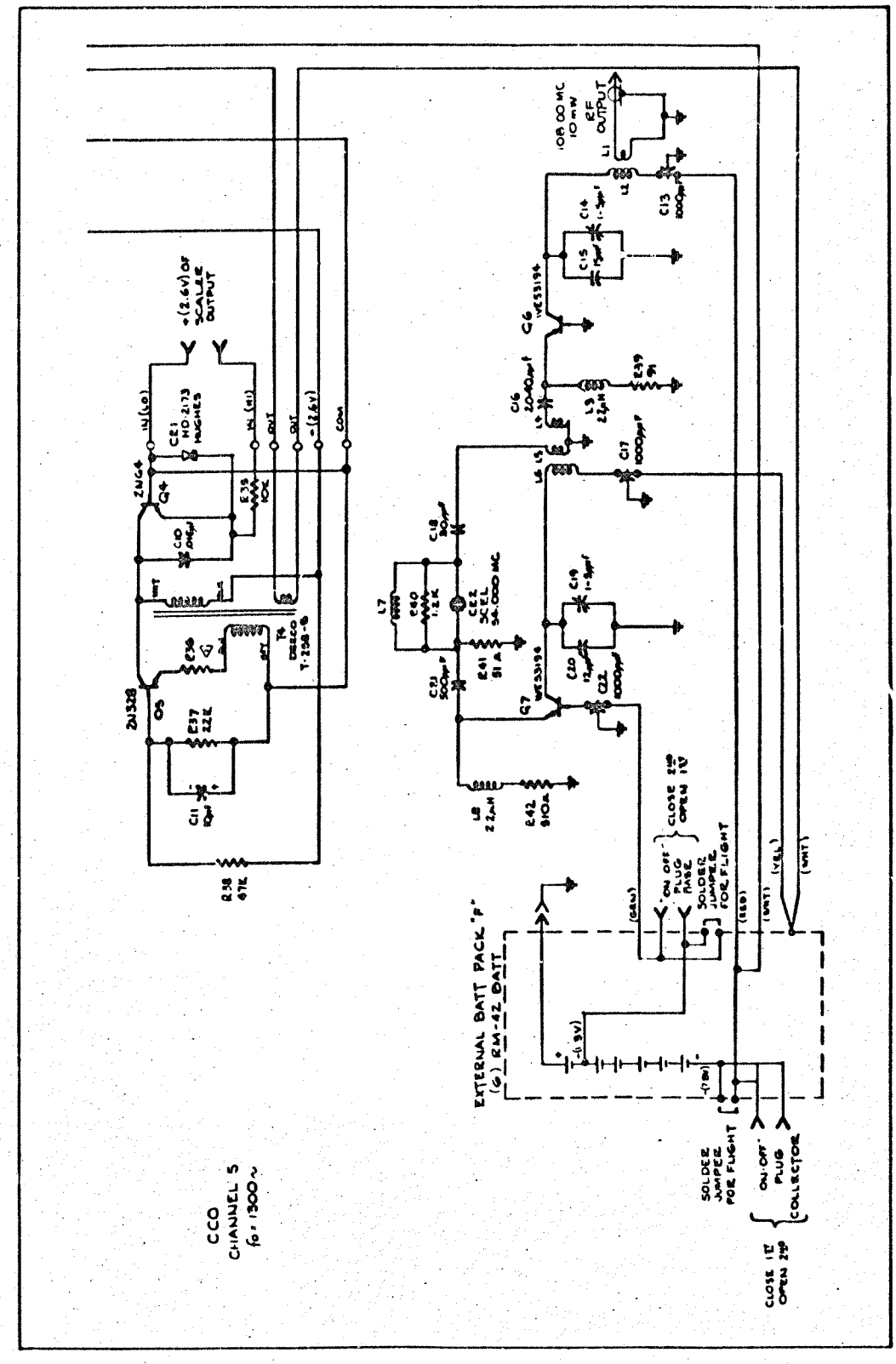

Fig. A-2. Schematic Diagram of Low-Power Transmitter

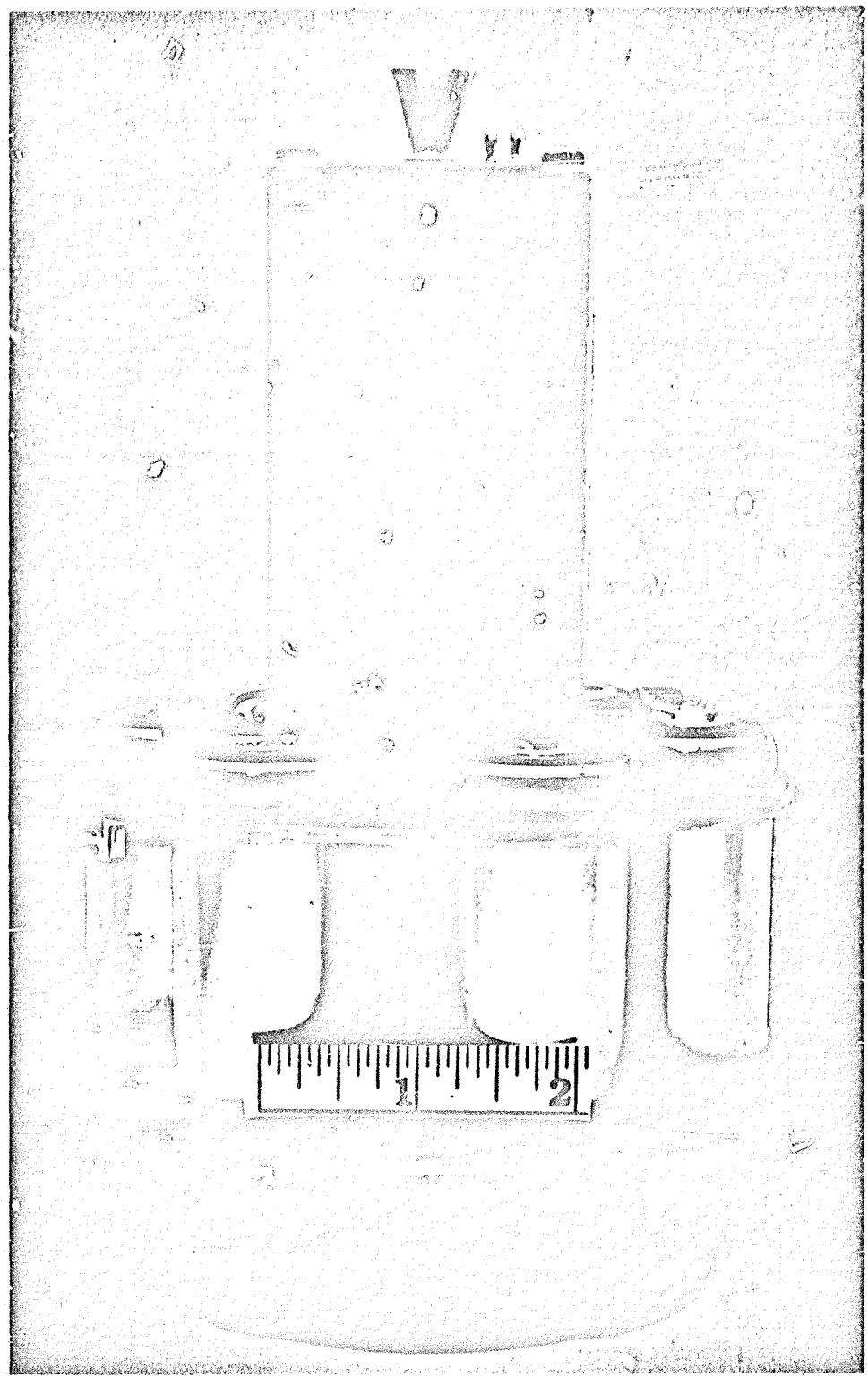

Fig. A-3. Photograph of Low-Power Beacon

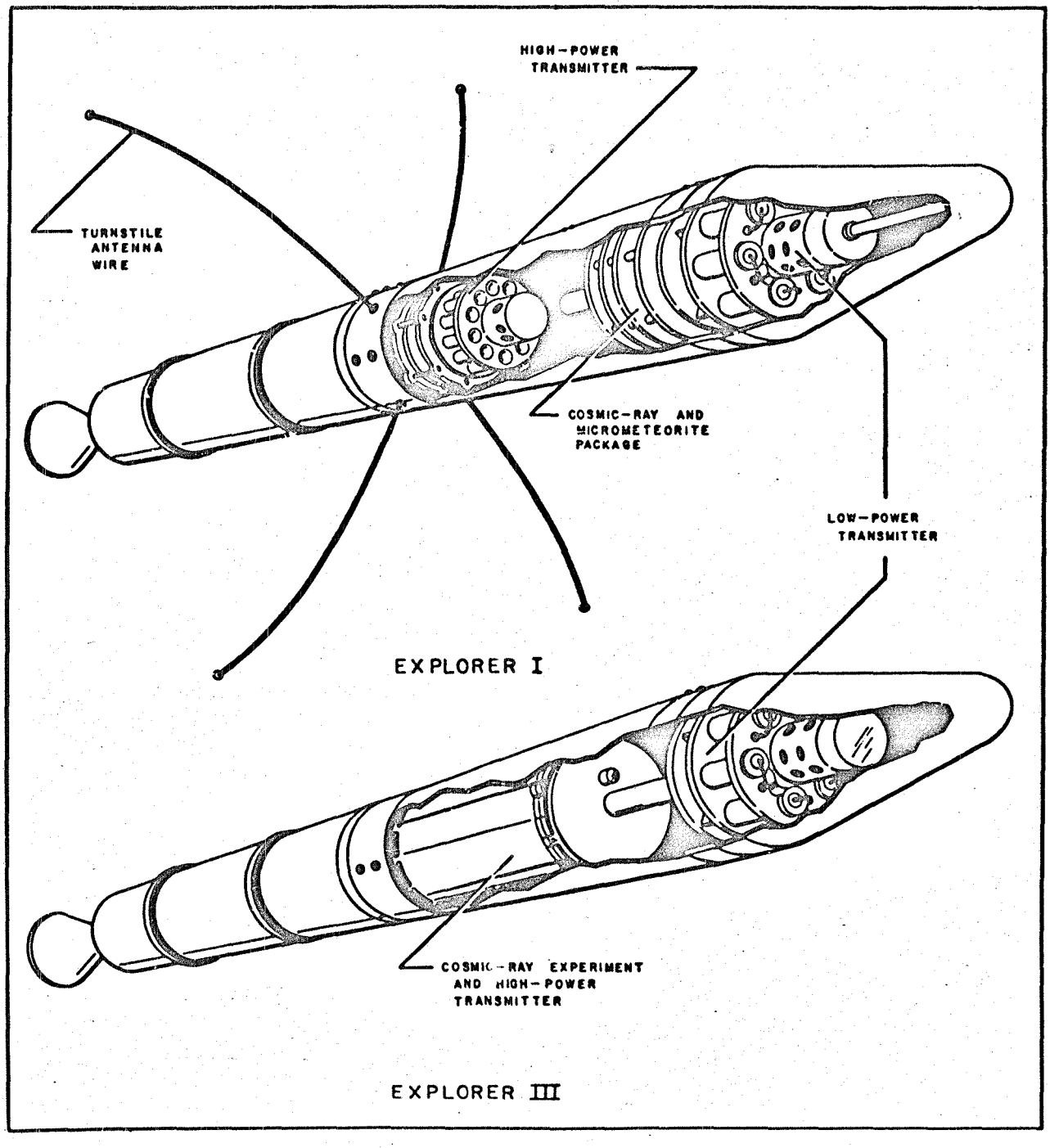

Fig. A-4. Cutaway View of Explorers I and III

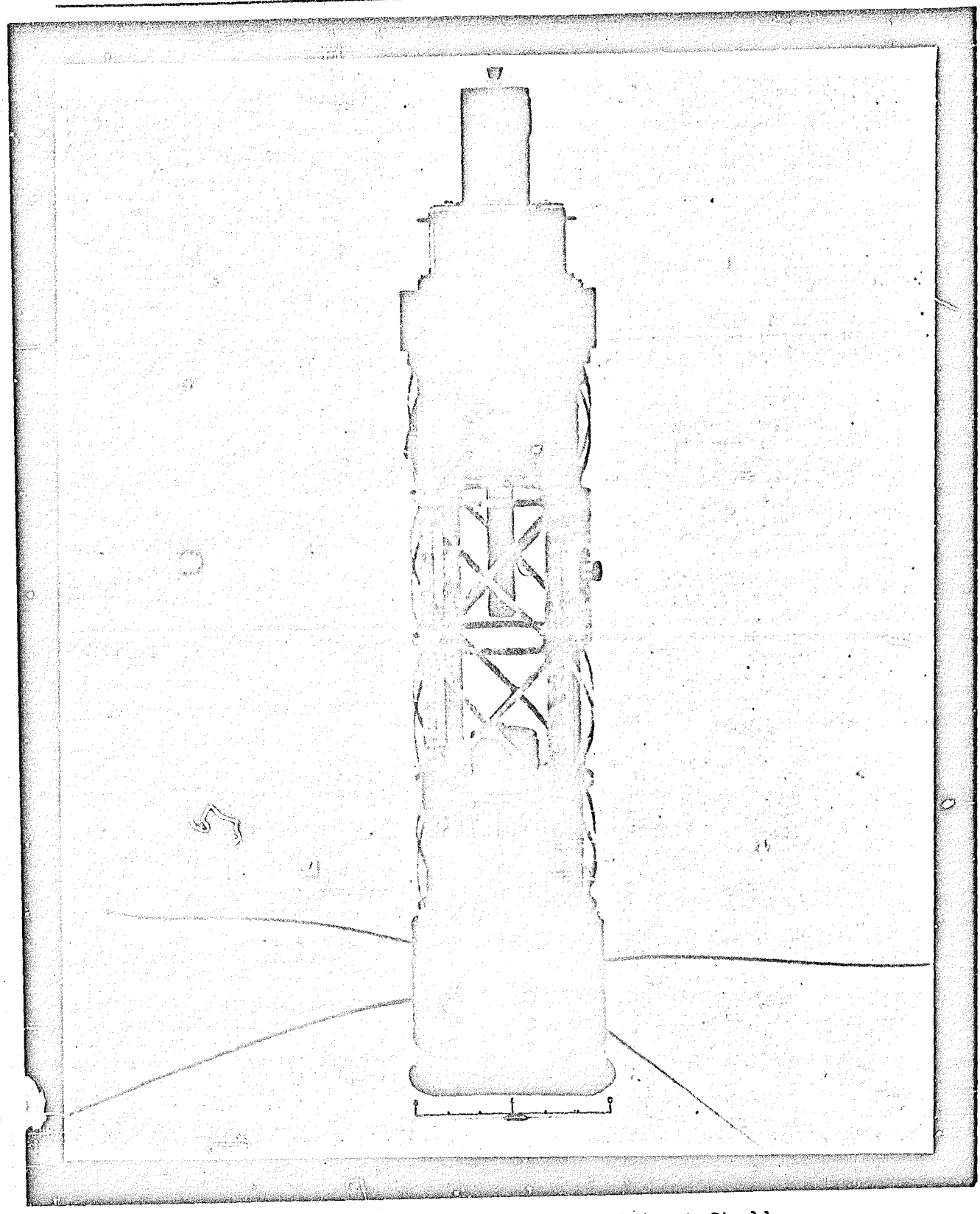

Fig. A-5. Explorer I Without Shell

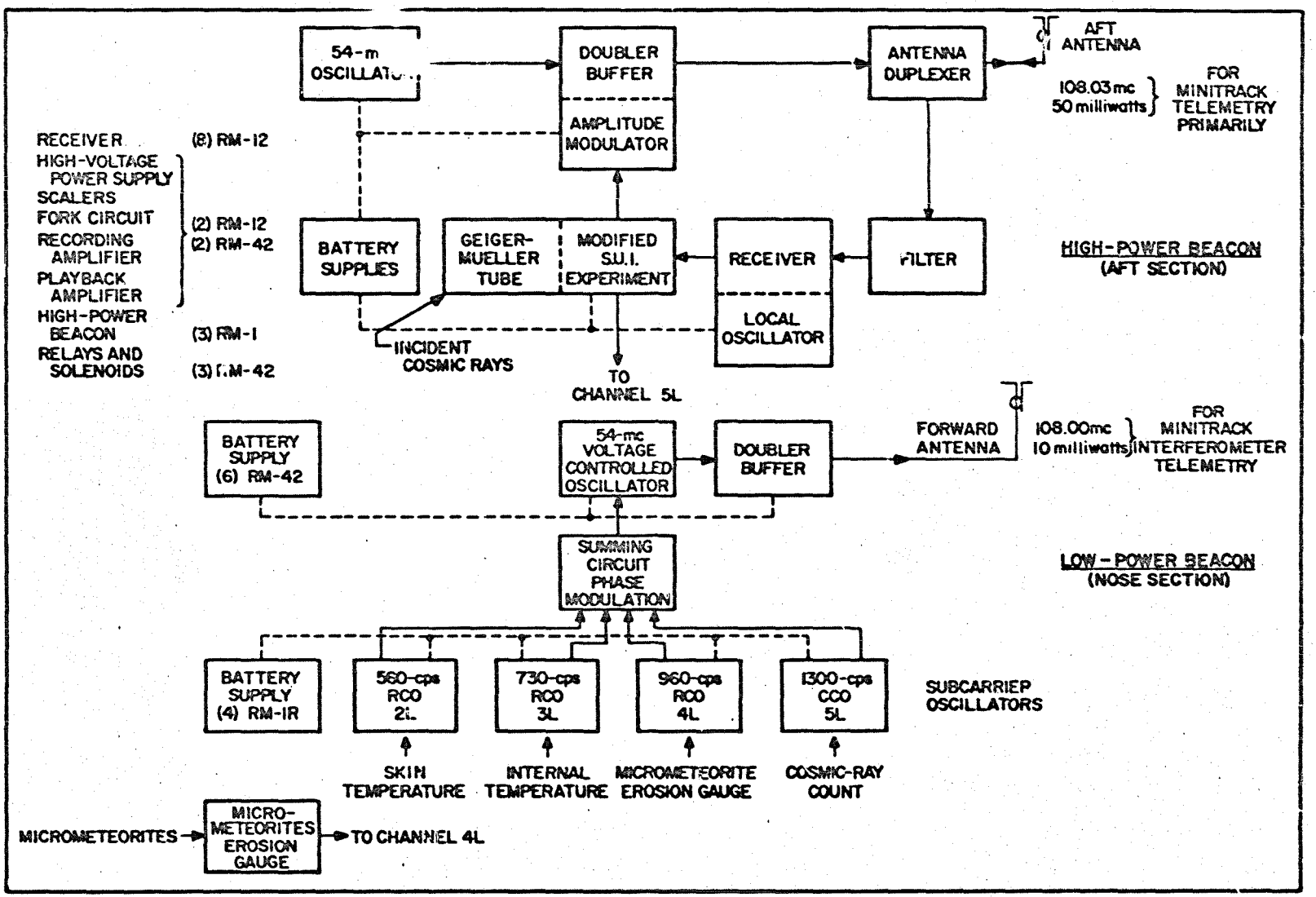

Fig. A-6. Block Diagram of Explorer III

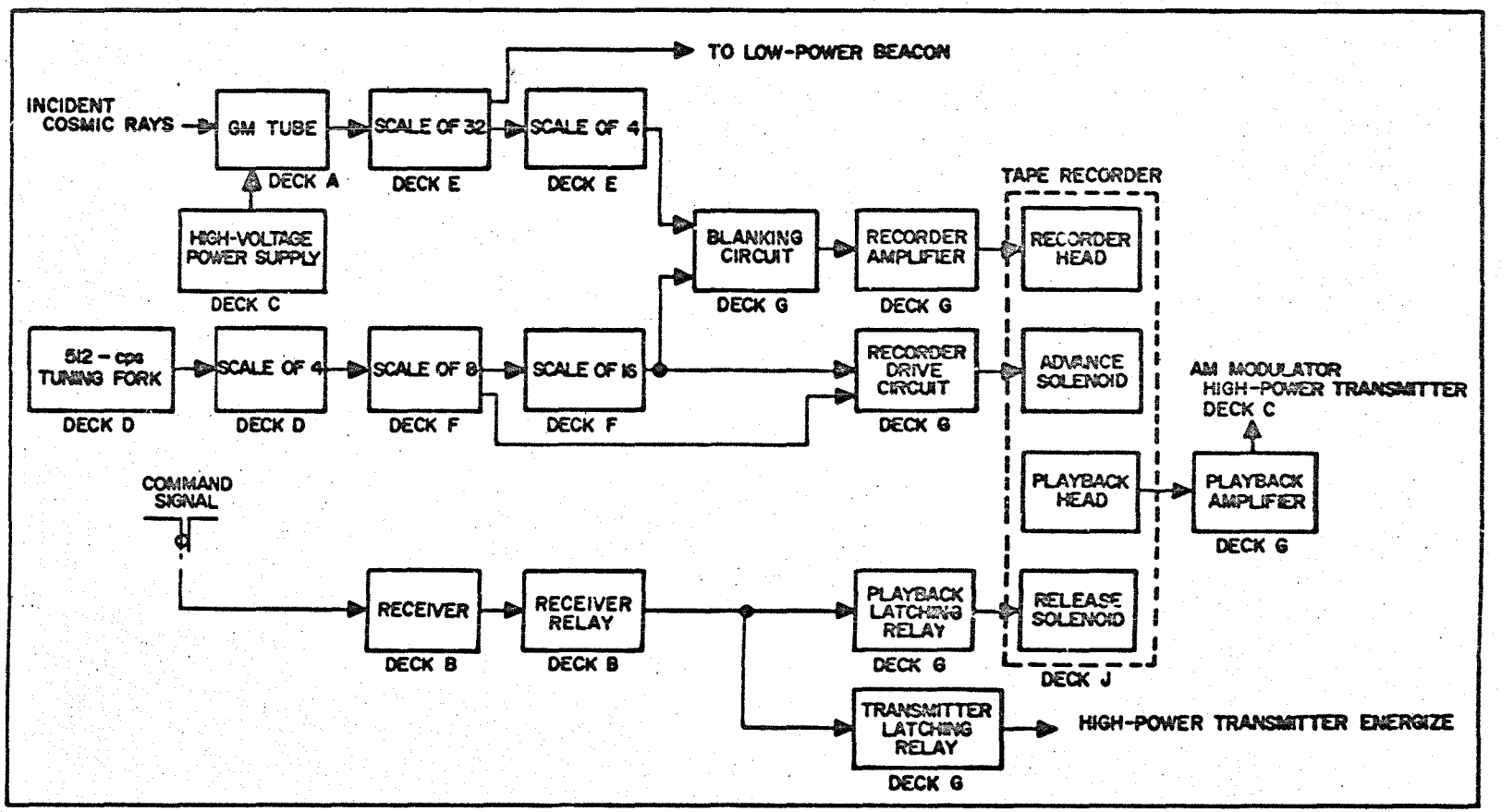

Fig. A-7. Block Diagram of Modified SUI Experiment

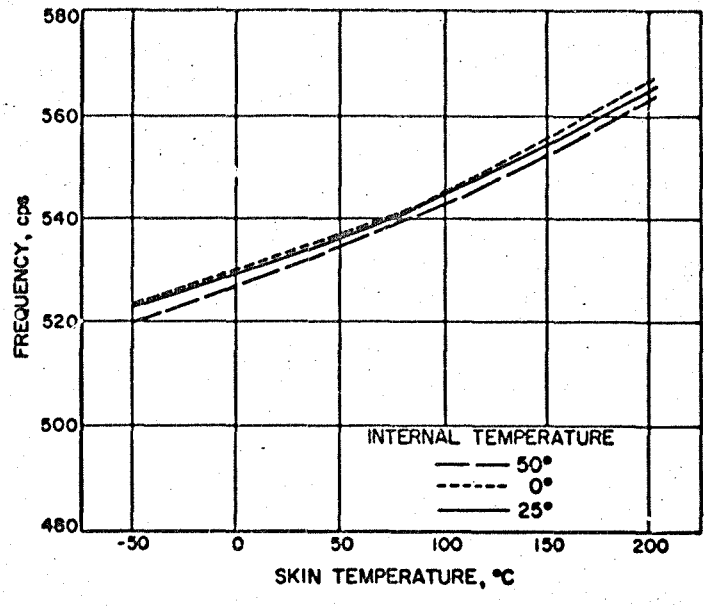

Fig. A-8. Calibration of Channel 2

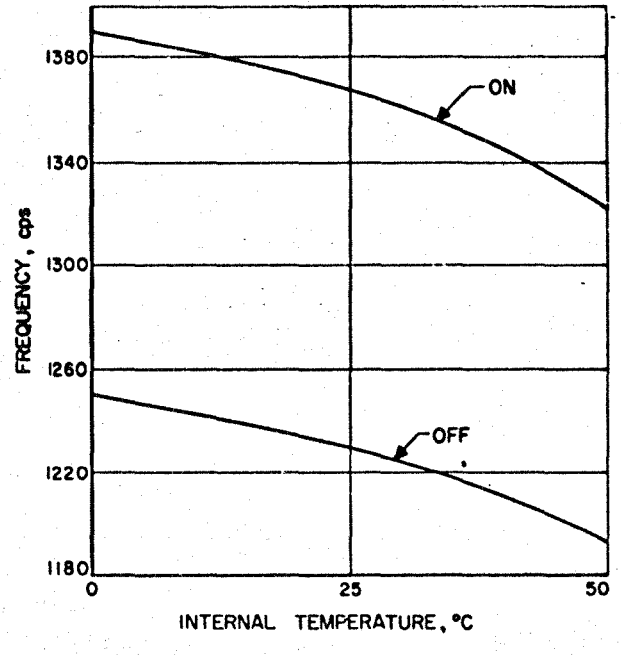

Fig. A-9. Calibration of Channel 5

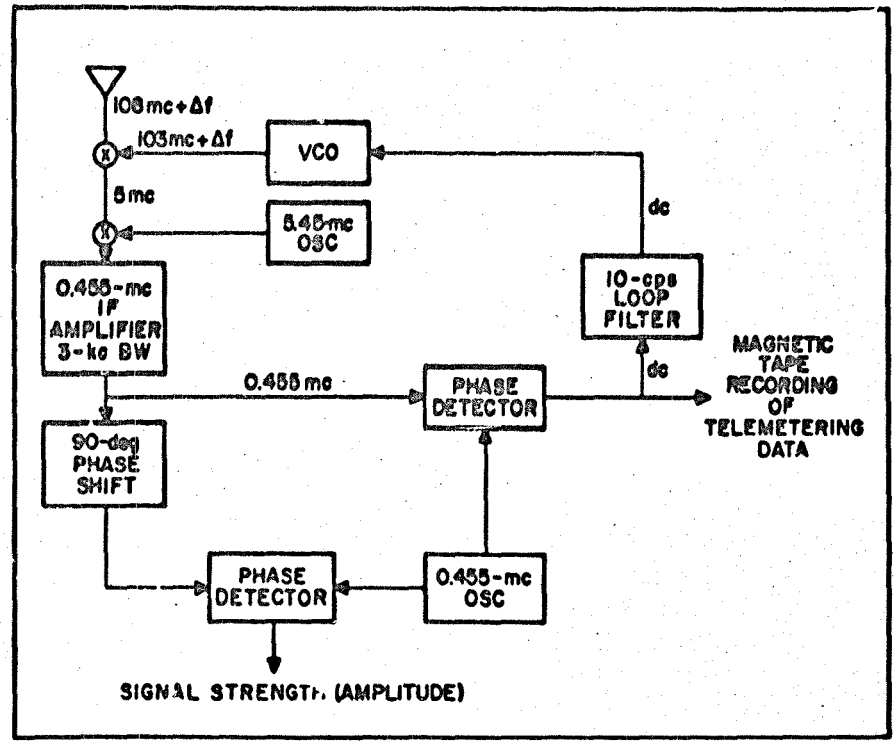

Fig. A-10. Simplified Block Diagram of Microlock Receiver

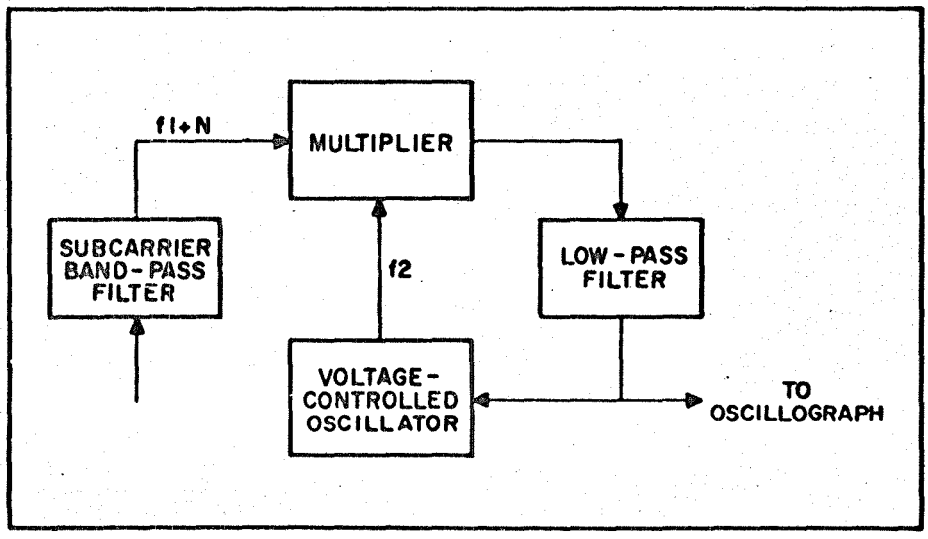

Fig. A-11. Simplified Block Diagram of Phase-Locked Discriminator

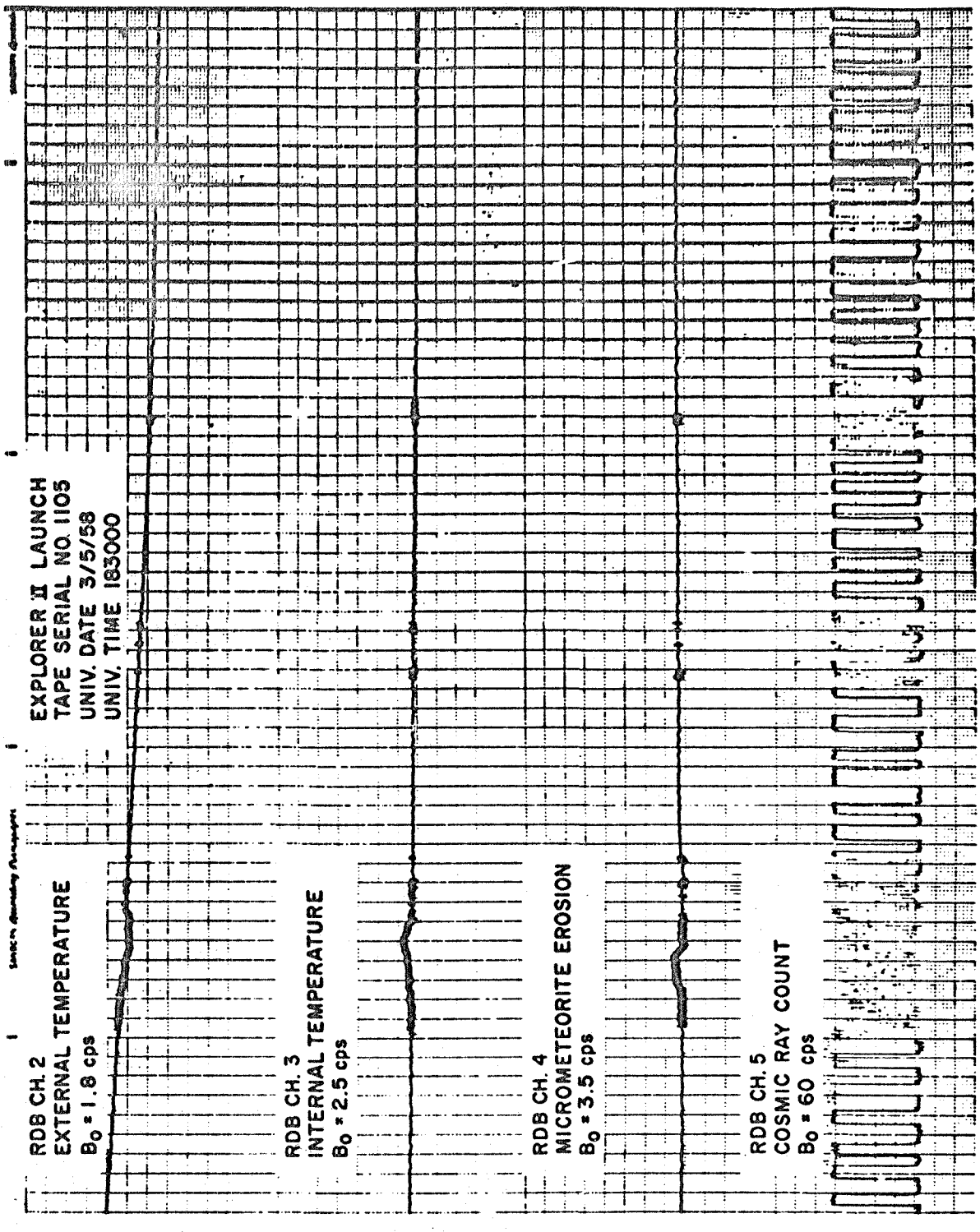

Fig. A-12. Section of Reduced Data

Appendix B. Explorer Antenna Patterns

Nomenclature

$E_\theta(\theta)$ = voltage in the θ direction as a function of θ.

$E_\varphi(\theta)$ = voltage in the φ direction as a function of θ.

φ, θ = angles as defined in Fig. B-1.

Explorer I Antenna Patterns

Figure B-1 shows the coordinate system used for describing the Explorer I RF radiation patterns. The longitudinal axis (axis of symmetry) of the satellite is oriented parallel to the z axis, with the nose of the model pointing in the positive z direction. The phase centers of the antennas are assumed to be at the center of the coordinate system.

Two antenna systems were used on Explorer I. The 108.00-mc transmitter drives a circumferential gap which is located roughly a tenth of a wavelength aft of the nose tip. The 108.03-mc transmitter drives a turnstile antenna located longitudinally at approximately the center of the satellite. The turnstile is composed of four quarter-wave flexible whips which, under the action of spin about the satellite longitudinal axis, form a system of two orthogonal half-wave dipoles. The plane described by these dipoles is parallel to the x - y plane as shown in Fig. B-1. The two dipoles are phased to provide dominantly right-hand circular polarization (IRE definition) in the aft hemisphere. The ellipticity is approximately 4 db along the symmetry axis. The following patterns are plotted in decibels.

The radiation pattern of the gap antenna is essentially independent of the φ coordinate. Figure B-2 is a polar plot of $E_\theta(\theta)$ for the front-gap antenna. The lack of symmetry may be attributed to ground reflections and other small errors incurred on our pattern range.

Figure B-3 shows the measured patterns of $E_\theta(\theta)$ measured in the $\varphi = 0°$ plane. Lack of symmetry of the measured pattern is considered to be measurement error due to range reflections. Patterns taken of $E_\varphi(\theta)$ were constant-amplitude, independent of θ, and therefore are not included.

Explorer II Antenna Patterns

The antenna patterns for Explorer II were essentially the same as the patterns for Explorer I. In Explorer II the low-power transmitter fed the front-gap antenna and the high-power transmitter (command operated) fed the turnstile antenna. The command-receiver antenna was a dipole formed by the motor case and the main body of the payload.

Explorer III Antenna Patterns

For Explorer III the whip antennas were removed. The low-power transmitter and antenna configuration at 108.00 mc was identical to Explorers I and II except that the front-gap impedance-matching network had to be retuned when the turnstile was removed. The rear gap was tuned to provide a reasonable impedance match at the 108.03-mc frequency and the frequency of the interrogation receiver, using a lumped-constant network. A simple duplexing network utilizing

critical interconnecting cables was provided to connect the command receiver and the high-power transmitter to the single gap antenna.

Two of the Explorer III antenna patterns are shown in Figs. B-4 and B-5. The Explorer IV and V patterns are essentially identical to those of Explorer III.

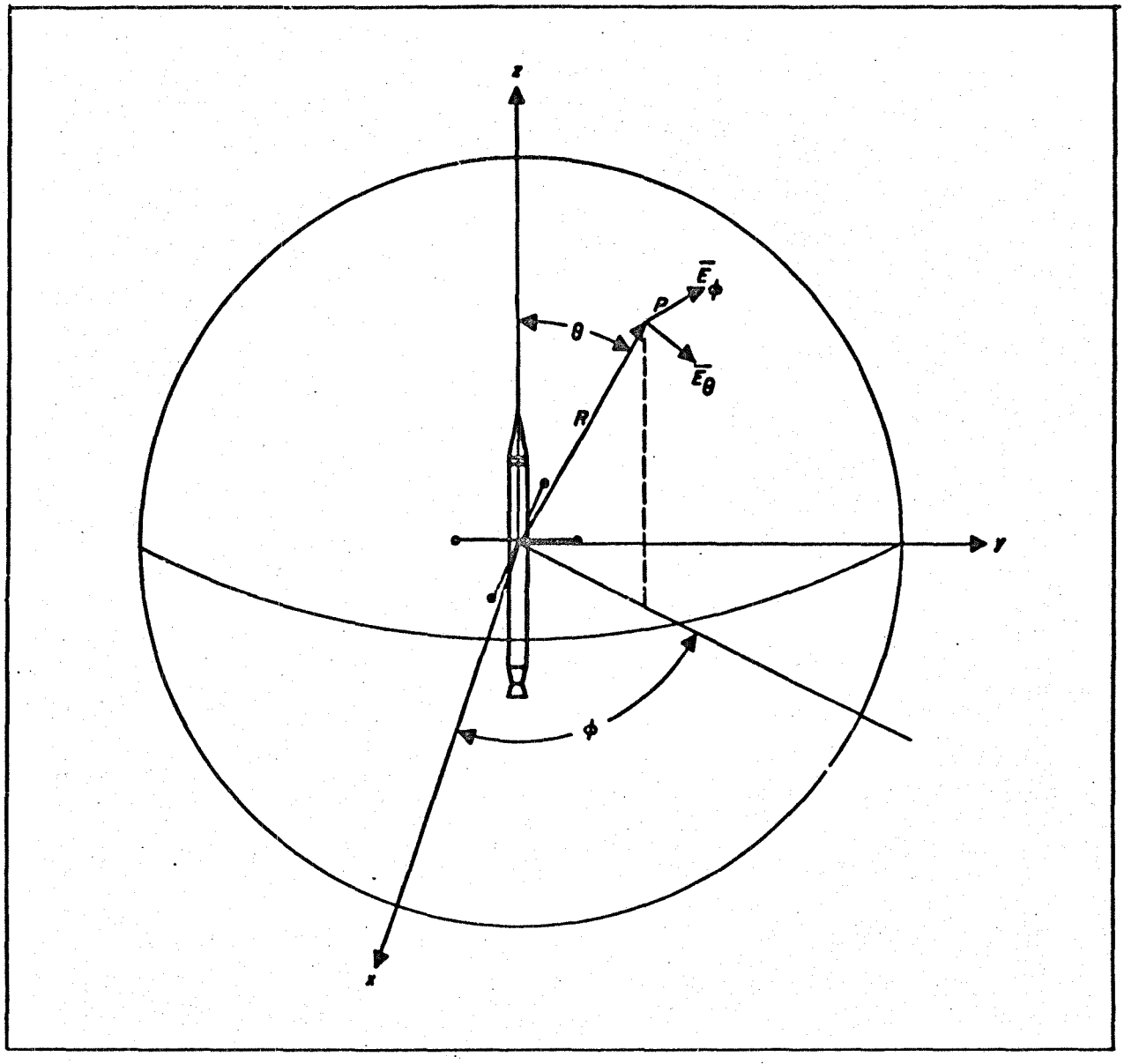

Fig. B-1. Coordinate System Used for Antenna Measurements

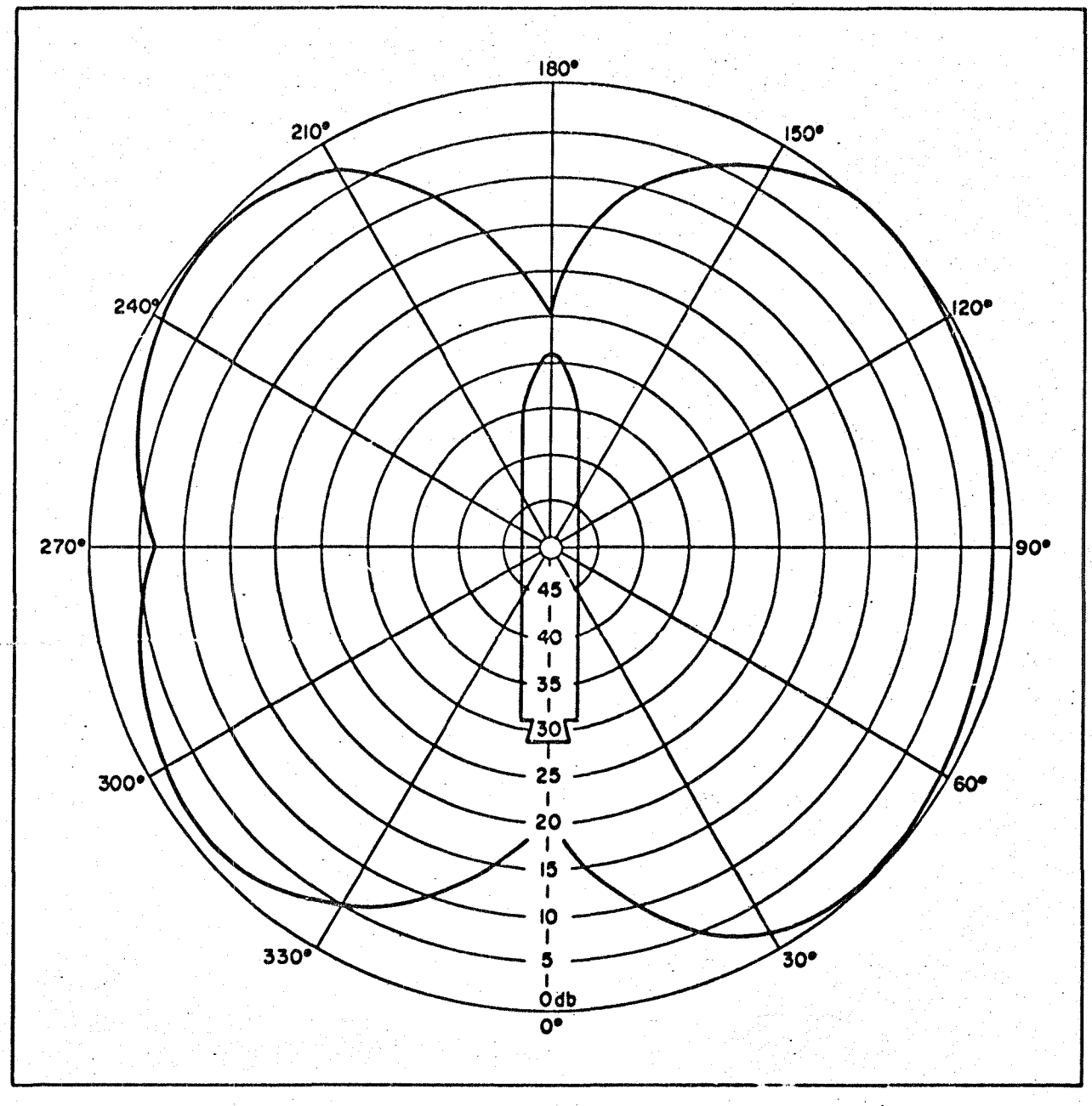

Fig. B-2. Plot of $E_\theta(\theta)$ for Explorer I 108.00-mc Front-Gap Antenna, Calibration in db, φ = 0 deg

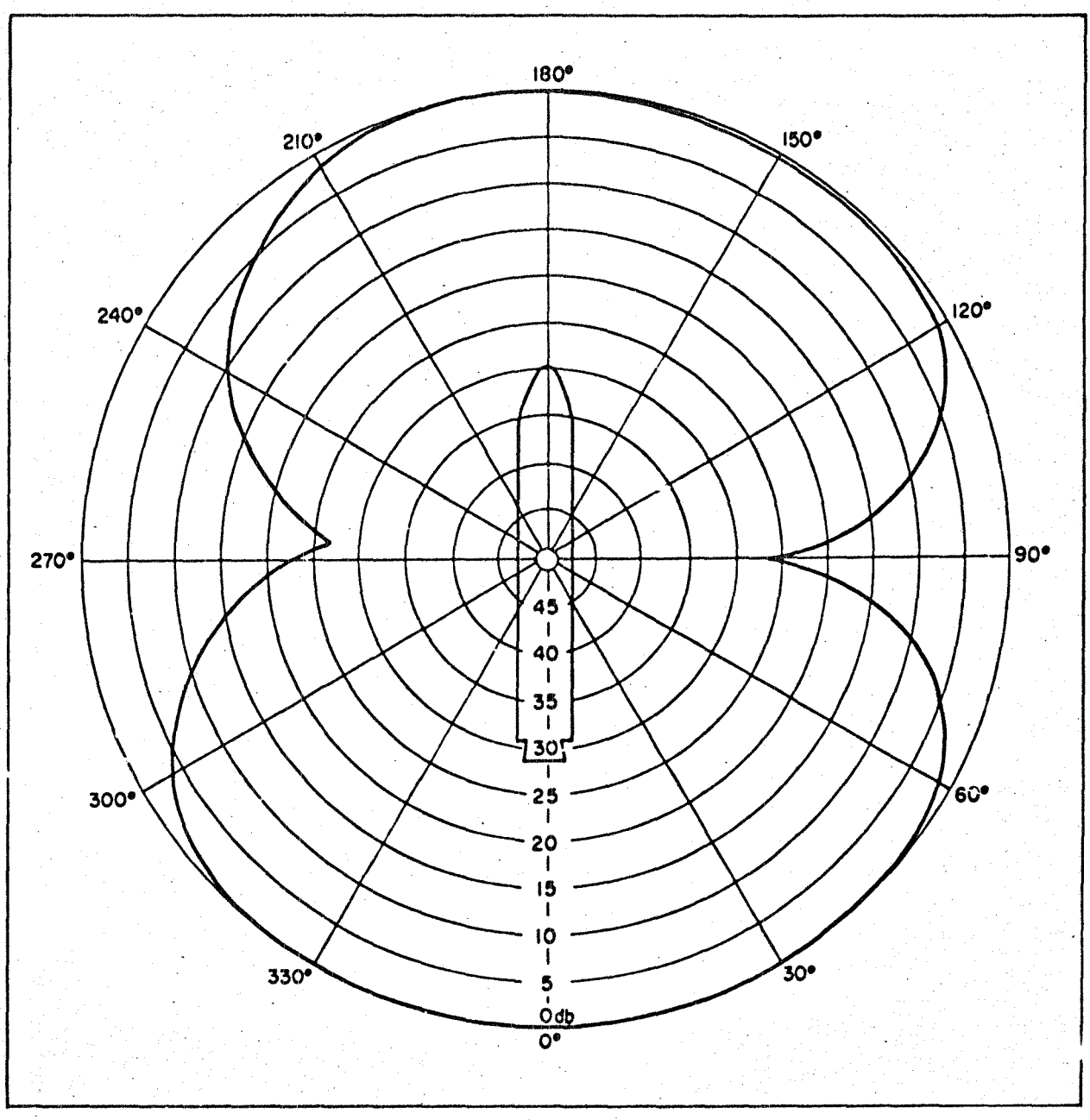

Fig. B-3. Plot of $E_\theta(\theta)$ for Explorer I 108.03-mc Turnstile Antenna, Calibration in db, φ = 0 deg

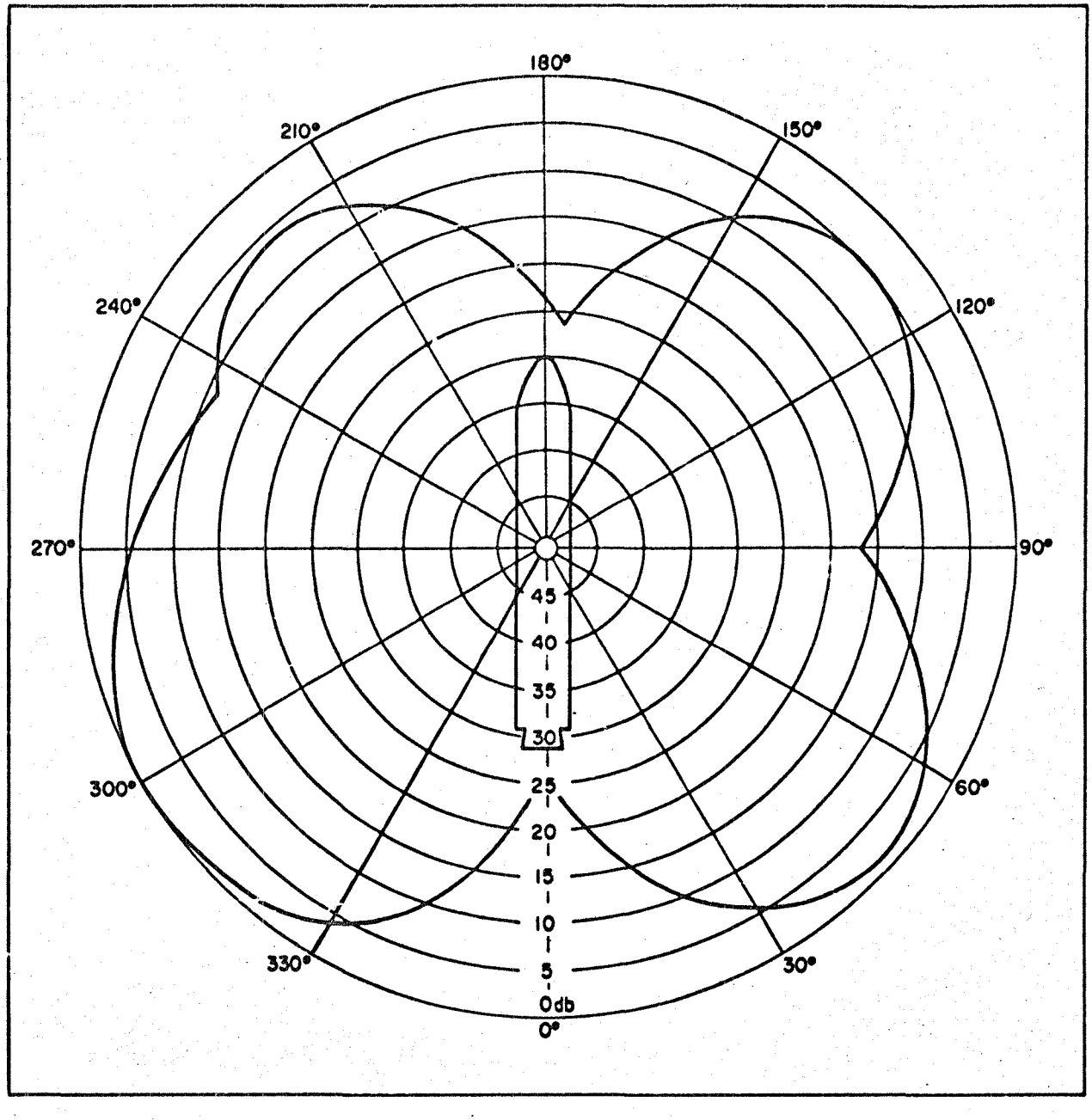

Fig. B-4. Plot of $E_\theta(\theta)$ for Explorer III 108.00-mc Front-Gap Antenna, Calibration in db, $\varphi = 0$ deg

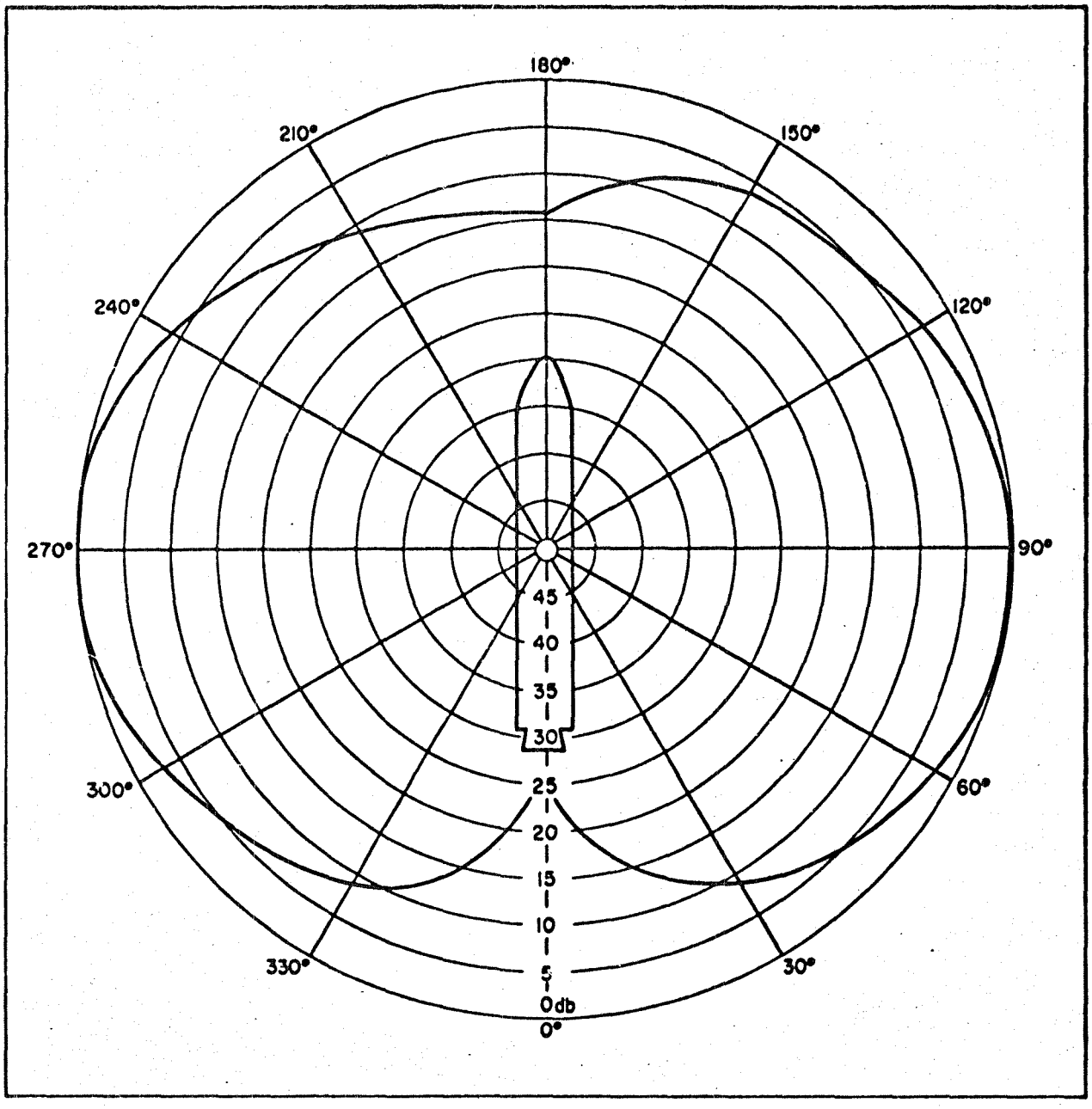

Fig. B-5. Plot of $E_\theta(\theta)$ for Explorer III 108.03-mc Rear-Gap Antenna, Calibration in db, φ = 0 deg

Appendix C. Spin Stability of Space Vehicles and the Tumbling of Explorer I[3]

NOMENCLATURE

a = pivot radius.

b = distance from plane of antenna pivots to center of mass of satellite.

B = a combination of constants, $m(a + c) + \rho ac/2 + \rho c^2/3$ (Eq. C-15).

c = antenna length.

CM = center of mass.

dm = increment of mass.

D = a combination of constants, $\left[a(m + \rho c/2)\right] 2B$ (Eq. C-16).

F = force.

$I_{1,2,3}$ = principal moments of inertia of rigid body.

L = angular momentum.

m = mass of swaging.

M_0 = torque amplitude.

p = the energy dissipated per cycle of bending per radian of amplitude squared.

r_φ = distance to $\dot{\varphi}$ axis.

r_ψ = distance to $\dot{\psi}$ axis.

s = distance along antenna wire from the effective pivot point.

T = kinetic energy.

$\vec{V}_r$ = velocity of dm in a rotating system.

x,y,z = coordinate axes in system rotation at $\dot{\varphi}$.

Z = complex amplitude of ζ.

---

[3]By Willard Wells, research engineer, Jet Propulsion Laboratory.

α = linear coefficient of restoring torque.

β = angle between symmetry axis and $\vec{\omega}$.

γ = linear coefficient of damping torque.

ζ = angle by which antenna bends aft.

η = angular amplitude.

θ = Euler angle, half-angle of precession cone.

ρ = linear density of the wire.

$\rho_{1,2,3}$ = coordinates along the principal axes.

τ = time during which satellite tumbles from θ_1 to θ_2.

$\dot{\vec{\varphi}}$ = precession rate.

φ, ψ = Euler angles.

$\dot{\vec{\psi}}$ = rotation rate, relative to a plane through $\vec{L}$ and the 3 axis.

ω = angular velocity.

Ω = 2π x driving frequency.

Ω_0 = 2π x resonant frequency.

Introduction

The rotation of a rigid body is stable if the body is rotating about the axis of least or greatest moment of inertia. If the body is nearly rigid, but has some part which moves slightly with friction, then only rotation about the axis of maximum moment is stable.

The purpose here is to study nearly rigid bodies and their rate of transition from rotation about any axis to stable rotation about the axis of maximum moment. Knowledge of this transition time is important in designing space vehicles which are required to have a stable attitude. In the case of a saucer-shaped vehicle, the transition time is the time required for the attitude to become fixed after some perturbation. In the case of cigar-shaped vehicles, such as the Explorers, the initial spin[4] about the symmetry axis is an unstable equilibrium. The transition time tells how quickly an operation requiring fixed attitude must be performed before tumbling sets in.

The general problem will be reduced to the following form. A formula will be derived for the forces which act on the frictional parts in terms of the parameters which describe the location of the frictional parts in the vehicle and the rotation of the vehicle as though it were rigid. From these forces the rate of energy dissipation must be found either theoretically or by reproducing the forces in the laboratory. The energy dissipation rate then goes into another formula (Eq. C-10) to give the slow rate of change of parameters which would be constant for a perfectly rigid body.

---

[4]The word spin will always refer to angular velocity about the symmetry axis; tumbling, to angular velocity at right angles to this axis.

Explorer I was a nearly rigid body rotating initially about its unstable axis of least moment. The most important frictional parts were the whip antennas. The change of Explorer I from unstable spin motion to the stable tumbling motion is analyzed as an example of the above method. The results agree well with radio data.

Rigid Body Motion

The motion of free rigid bodies is derived in many mechanics texts (Refs. 2, 3). The results of the derivation will be summarized here. Let I_1, I_2, and I_3, be the principal moments of inertia of the rigid body. In the case of a symmetrical body, I_3 is the moment about the symmetry axis and $I_1 = I_2$. The body will be represented by its so-called ellipsoid of inertia (Ref. 2) which is long or short in the same general directions as the mass distribution of the body it represents. Thus, the ellipsoid for Explorer I is cigar-shaped. The equation of the ellipsoid is

$$1 = I_1 \rho_1^2 + I_2 \rho_2^2 + I_3 \rho_3^2$$

where ρ_1, ρ_2, and ρ_3 are coordinates along the principal axes. The ellipsoid intercepts the principal axes at distances $I_1^{-1/2}$, $I_2^{-1/2}$, and $I_3^{-1/2}$. For Explorer I, these are in the ratio of about 1,1,8.7. Imagine the body contained in the ellipsoid and rigidly attached so that the center of mass (CM) lies at the center of the ellipsoid, and the principal axes coincide. Then the motion of the ellipsoid gives the motion of the body. The most general motion is as follows: the ellipsoid rolls without slipping on a plane while its center is fixed. The angular momentum vector $\vec{L}$ is perpendicular to the plane as shown

in Fig. C-1. The angular velocity vector $\vec{\omega}$ passes through the CM and the point of contact with the plane, since these points are stationary. While $\vec{L}$ is fixed in space, $\vec{\omega}$, in general, changes direction in both body and space fixed coordinates. This is possible because

$$\vec{L} = I_1\vec{\omega}_1 + I_2\vec{\omega}_2 + I_3\vec{\omega}_3$$

so that $\vec{L}$ can be formed from different amounts of $\vec{\omega}_1$, $\vec{\omega}_2$, and $\vec{\omega}_3$, depending on the I's and the orientation of the body.

Until otherwise stated, from now on only the symmetric case $I_1 = I_2$, will be considered. The ellipsoid becomes a figure of revolution, the 3 axis being the symmetry axis. In this case, Fig. C-1 shows that the 3 axis precesses in a circular cone of half-angle θ, while $\vec{\omega}$ precesses in a circular cone of half-angle $\theta-\beta$.

This is the same motion as is obtained if the body is represented by a cone (Ref. 3) of half-angle β rolling around a space cone of half-angle $\theta-\beta$ with vertices coinciding as shown in Fig. C-2. This representation will be used later. Figure C-2 also shows the vector $\vec{\omega}$ resolved into $\vec{\dot{\varphi}}$, the precession rate, and $\vec{\dot{\psi}}$, the rotation rate relative to a plane through $\vec{L}$ and the 3 axis.[5] The notation ψ, φ, and θ refers to Euler angles (Ref. 2, p. 107, or Ref. 3, p. 108). The quantities in Fig. C-2 are related through the moments of inertia by (Ref. 3, p. 112)

$$\dot{\varphi}\cos\theta = \frac{I_3}{I_1}\omega_3 \qquad \text{(C-1)}$$

[5]The distinction between $\dot{\psi}$ and $\dot{\psi} + \dot{\varphi}$ is analagous to solar and sidereal time, respectively.

$$\dot{\psi} = \frac{I_1 - I_3}{I_1} \omega_3 \qquad \text{(C-2)}$$

where $\omega_3 = \dot{\psi} + \dot{\varphi} \cos \theta$. For Explorer I, $\dot{\varphi}$ and ω_3 were observed directly from intensity fluctuations in the radio signals. Knowing these, Eq. (C-1) relates θ to the moment of inertia ratio.[6] Using the triangles of Fig. C-2, it is easily shown that

$$\tan \beta = \frac{I_3}{I_1} \tan \theta \qquad \text{(C-3)}$$

For Explorers I and III, I_3/I_1 was about 75. In this case, Eq. (C-3) shows that β is a small angle until the satellite tumbles to an angle θ very near to 90 deg (arctan 75). This checks with Fig. C-1 for the case in which the major axis is 8.7 times ($\sqrt{75}$ x) the minor axis. Since the last few degrees of tumbling are not very interesting, the approximation $\beta \ll 1$ radian will be used.

Nearly Rigid Body Motion

If a body is nearly rigid, the effects of frictional parts will be very small during one period of precession ($2\pi/\dot{\varphi}$). Therefore, the rapid motion will still be described by the rolling ellipsoid of Fig. C-1. The only remaining part of the description of motion which may be changed by friction is the spin rate and the parameters which describe the cone of precession; that is, the cone of half-angle θ, which the 3 axis traces out.[7] Since there are no external forces,

[6] Eq. (C-1) Applies to nearly rigid bodies also.

[7] Looking at Fig. C-2, one might think both body and space cones can change angle, but these are related by Eq. (C-3). It can be seen in Fig. C-1, that there is no problem because β and θ are related by the shape of the ellipsoid which does not change permanently, although it does vibrate slightly as the frictional part moves.

the vector $\vec{L}$ is constant. Therefore, the orientation of the precession cone does not change, since its axis is parallel to $\vec{L}$. This leaves only θ and ω to change, but ω is determined by the constant magnitude of L when θ is given, the equations being

$$\begin{aligned} L_3 &= L \cos\theta = \omega_3 I_3 \\ L_1 &= L \sin\theta = \omega_1 I_1 \end{aligned} \qquad \text{(C-4)}$$

Thus, θ is the only quantity for which an equation of motion must be found and integrated. It is also a convenient quantity, since it is the most obvious one to measure when looking at a precessing body.

For the important case in which θ is initially zero, and ω initially ω_0, it is convenient to express ω_3 in terms of ω_0, and θ. By Eq. (C-4),

$$\omega_3 = \frac{L \cos\theta}{I_3} = \omega_0 \cos\theta \qquad \text{(C-5)}$$

Substituting Eq. (C-5) in Eqs. (C-1) and (C-2) gives

$$\dot{\varphi} = \frac{I_3}{I_1}\omega_0 \qquad \text{(C-6)}$$

$$\dot{\psi} = \frac{I_1 - I_3}{I_1}\omega_0 \cos\theta \qquad \text{(C-7)}$$

Note that $\dot{\varphi}$ is a constant of the motion. For Explorer I this is confirmed by radio data.

A first-order differential equation for θ is found simply by conserving energy and momentum. The kinetic energy T may be expressed in terms of L and θ as

$$T = \frac{L_1^2}{2I_1} + \frac{L_3^2}{2I_3} = \frac{L^2}{2}\left(\frac{\sin^2\theta}{I_1} + \frac{\cos^2\theta}{I_3}\right) \qquad \text{(C-8)}$$

The only variables in Eq. (C-8) are T and θ. The quantity T decreases as energy is dissipated, changing θ, at a rate given by the derivative of Eq. (C-8).

$$\frac{d\theta}{dT} = \left(\frac{dT}{d\theta}\right)^{-1} = \left[\frac{L^2}{2}\sin 2\theta\left(\frac{1}{I_1} - \frac{1}{I_3}\right)\right]^{-1} \qquad \text{(C-9)}$$

Since T decreases, Eq. (C-9) says that θ increases if $I_1 > I_3$ and θ decreases if $I_3 > I_1$. In both cases, $\vec{\omega}$ tends toward the axis of largest moment of inertia. In other words, the spin of a saucer-shaped body is stable, but that of a cigar-shaped nearly rigid body is unstable and changes to a tumbling[3] motion.

To form the differential equation in terms of θ only, one can substitute Eq. (C-9) into the identity

$$\frac{d\theta}{dt} = \frac{d\theta}{dT}\frac{dT}{dt}$$

obtaining

$$\frac{d\theta}{dt} = 2\frac{dT}{dt}\left[L^2 \sin 2\theta\left(\frac{1}{I_1} - \frac{1}{I_3}\right)\right]^{-1} \qquad \text{(C-10)}$$

Equation (C-10) is one of the general formulas mentioned in the introduction. The others which will be derived presently (Eqs. C-11, C-12) give the forces on the frictional parts which result from constraining them to ride the ellipsoid of Fig. C-1. Then generality

ends. The forces must be applied to the specific frictional parts to find the rate at which they dissipate energy. This rate, which equals $-dT/dt$, is a function of θ through the forces. Substituting $dT(\theta)/dt$ into Eq. (C-10) gives a first-order differential equation with variables θ and t which separate.

Care must be taken in finding the forces which cause acceleration of the frictional parts relative to their supports, because the supports accelerate also in executing the motion described by the rolling ellipsoid. The force which causes the parts to merely keep up with their supports cannot produce any friction and must not be included. To avoid trouble of this type, the coordinate system shown in Fig. C-3 will be used. The origin is at the CM. The z axis is the symmetry axis, and the x axis lies in the plane containing $\vec{L}$, and the symmetry axis. In this system the vehicle merely rotates about the z axis with frequency $\dot{\psi}/2\pi$, so that the only acceleration of the supports is centripetal. Since this coordinate system is not inertial but is rotating with angular velocity $\dot{\varphi}$, there will be, in addition to the centrifugal force proportional to $\dot{\psi}^2$, a coriolis force proportional to $\dot{\psi}\dot{\varphi}$, and a centrifugal force proportional to $\dot{\varphi}^2$.

The centrifugal forces acting on the small mass dm in Fig. C-3 are

$$F_\psi = dm\, \dot{\psi}^2\, r_\psi$$
$$F_\varphi = dm\, \dot{\varphi}^2\, r_\varphi \qquad \text{(C-11)}$$

where $r_\psi = \sqrt{x^2 + y^2}$ is the distance to dm from the symmetry or $\dot{\psi}$ axis, and r_φ is the distance from the $\dot{\varphi}$ axis. The force F_ψ is steady.

The quantity F_φ is time-varying with frequency $\dot{\psi}/2\pi$; but for the case of a cigar-shaped vehicle, F_φ is negligible, since $\dot{\psi}^2$ is of the order of $10^4\dot{\varphi}^2$.

The coriolis force on dm in a coordinate system rotating with angular velocity $\vec{\dot{\varphi}}$ is given by (Ref. 2, p. 135) 2 dm $\vec{v}_r \times \vec{\dot{\varphi}}$, where $\vec{v}_r$ is the velocity of dm in the rotating system. The magnitude of $v_r = \dot{\psi} r_\psi$. The angular dependence in the cross product is time-varying with frequency $\dot{\psi}/2\pi$. The origin of time is chosen when dm is in the x-z plane, as shown in Fig. C-3.

Then, by studying the angles in Fig. C-3, it is easy to show that the coriolis force coupling $\dot{\varphi}$ and $\dot{\psi}$ is given by

$$\begin{aligned} F_{\varphi\psi r} &= 2\ dm\ \dot{\psi}\dot{\varphi} r_\psi \cos\theta \\ F_{\varphi\psi z} &= -2\ dm\ \dot{\psi}\dot{\varphi} r_\psi \sin\theta \cos(\dot{\psi}\ t) \end{aligned} \qquad \text{(C-12)}$$

where $F_{\varphi\psi r}$ is the component in the r_ψ direction (x-y plane), and $F_{\varphi\psi z}$ is the z component. The force $F_{\varphi\psi r}$ is steady; $F_{\varphi\psi z}$ is the principal sinusoidal driving force which causes the energy dissipation. Coriolis force resulting from the motion of parts relative to their supports can usually be neglected, and will be for the Explorer example which follows.

Equations (C-10), (C-11), and (C-12) complete the general treatment of nearly rigid bodies.

Tumbling of Explorer I

The tumbling of Explorer I will now be solved as an example of the theory just derived. The antennas act as damped driven pendulums. It happens that the driving force is very nearly resonant in this

case, making a very effective damper. This near resonance makes it necessary to include the elastic restoring force of the wire, even though it is very small compared to centrifugal restoring force. Since the natural frequency depends upon the restoring force, the effect of a small additional restoring force on the amplitude of oscillation is greatly magnified by the subtraction in a typical resonance denominator of the form (driving frequency)^2 - (resonant frequency)^2 + i(damping term).

The accuracy of the elastic restoring torque limits the accuracy of the whole calculation to about 30%, for two reasons. First, some antennas wobble slightly in their supports without bending. Second, the exact configuration into which the wire bends under centrifugal force is difficult to reproduce in the laboratory. The configuration changes as the spin decays, and the restoring torque may depend nonlinearly on the bend angle. A simple linear value of restoring torque will be used here. It was obtained by the following method. First, an ordinary pendulum was made of antenna wire with a heavy pendulum bob to imitate the centrifugal force at 10 cps. The bending radius of this pendulum was estimated. Then small weights were hung on a piece of antenna wire, one end of which was held horizontally in a vice. When the weights were adjusted so that the same bending radius was obtained for a small bending angle, the torque was calculated and divided by the angle to give the linear coefficient.

Equations (C-11) and (C-12) are used to calculate the pendulum amplitude. The quantities F_{ψ} ano $F_{\varphi\,\psi r}$ provide the restoring constraint force. The driving force is $F_{\varphi\psi\,z}$; F_{φ} is negligible. The quantities a, b, and c in Fig. C-4 describe the antenna position

and length. The wire has a linear density ρ and swaging on the end with mass m. The wire is treated as a straight rod pendulum on a point pivot. The fact that the wire really has a bending radius is accounted for by the added restoring force and a slight adjustment in a, the pivot radius. Instead of measuring a to the surface of the satellite, it was measured to the intersection of the line tangent to the antenna at its midpoint, with the radial line through the antenna support. Since there is no driving force in the x - y plane,[8] there is no steady-state motion of the antenna in the transverse direction and, hence, no need for a variable to describe transverse position. The motion of one of the antennas will be solved using a single variable ζ, the angle by which the antenna bends aft (+z direction).

The equation of motion for ζ is found by equating the sum of the torques to $\ddot{\zeta}$ times the moment of inertia of the antenna. The linear coefficients of damping and restoring torques are defined to be γ and α, respectively. That is, $\gamma\dot{\zeta}$ is the damping torque, and $\alpha\zeta$ the restoring torque. The antenna's moment of inertia is $\int_0^c \rho s^2 ds + mc^2$, where s is distance along the wire from the effective pivot point. Torques must be calculated by substituting the quantities m, ρ, a, and c in Eqs. (C-11) and (C-12). For example, the coriolis part of the restoring force is given by the $\sin\zeta \approx \zeta$ component of

---

[8]The neglected centrifugal force due to $\dot{\varphi}$ has a small component proportional to $\dot{\varphi}^2 b \sin\theta\cos\theta$ driving the antenna in the transverse direction at the frequency $\dot{\psi}/2\pi$. If the restoring forces in the two directions were such that the transverse was much more nearly resonant than the longitudinal, then transverse oscillations might dominate despite their small driving force; but, in fact, the opposite is true.

$F_{\psi\psi r}$ of Eq. (C-12). This force acting on the swaging is $2m\dot{\psi}\dot{\varphi}(a+c)(\cos\theta)\zeta$. Acting on an increment of wire, it is $2\rho ds\,\dot{\psi}\dot{\varphi}(a+s)(\cos\theta)\zeta$. After multiplying by the lever arms and integrating, the coriolis part of restoring torque is found to be $2m\dot{\psi}\dot{\varphi}(a+c)c(\cos\theta)\zeta + \int_0^c 2\rho\dot{\psi}\dot{\varphi}(a+s)s(\cos\theta)\zeta\,ds$. Putting all the pieces together gives the following equation of motion:

$$-\left[m\dot{\psi}^2(a+c)c + \int_0^c \rho\dot{\psi}^2(a+s)\,sds\right]\zeta$$

$$-\left[2m\dot{\varphi}\dot{\psi}(a+c)c + 2\int_0^c \rho\dot{\psi}\dot{\varphi}(s+a)\,sds\right]\cos\theta\,\zeta$$

$$+\left[2m\dot{\varphi}\dot{\psi}(a+c)c + 2\int_0^c \rho\dot{\varphi}\dot{\psi}(s+a)\,sds\right]\sin\theta\cos(\dot{\psi}t)$$

$$-\gamma\dot{\zeta} - \alpha\zeta = \left[mc^2 + \int_0^c \rho s^2 ds\right]\ddot{\zeta} \qquad \text{(C-13)}$$

Performing the integrations and some algebra results in

$$\left(mc + \frac{\rho c^2}{3}\right)\ddot{\zeta} + \left(\frac{\gamma}{c}\right)\dot{\zeta} + \left(\frac{\alpha}{c}\right)\zeta \qquad \text{(C-14)}$$

$$+B(\dot{\psi} + 2\cos\theta\,\dot{\varphi})\dot{\psi}\zeta = 2B\sin\theta\dot{\varphi}\dot{\psi}\cos(\dot{\psi}t)$$

where

$$B = m(a+c) + \frac{\rho ac}{2} + \frac{\rho c^2}{3} \qquad \text{(C-15)}$$

To solve this by complex numbers in the usual manner for a linear equation, let $\zeta = \mathrm{Re}\,Ze^{i\dot{\psi}t}$, $\cos(\dot{\psi}t) = \mathrm{Re}\,e^{i\dot{\psi}t}$. Then Eq. (C-14) can be solved for the complex amplitude Z.

$$Z = \frac{\tan\theta}{1 + D(R-1) + \dfrac{i\gamma R}{2B\,c\,\omega_0\cos\theta} + \dfrac{R^2\alpha}{2(R-1)\,\omega_0^2\cos^2\theta}} \qquad \text{(C-16)}$$

where

$$D = \frac{a\left(m + \frac{\rho c}{2}\right)}{2B}$$

$$R = \frac{I_1}{I_3}$$

and Eqs. (C-6) and (C-7) have been used to eliminate $\dot{\varphi}$ and $\dot{\psi}$.

The damping constant γ which appears in Eq. (C-16) must be evaluated for the wire used in the whip antennas. First, the quantity $2\pi p$ is defined as the energy dissipated per cycle of bending per radian of amplitude squared; that is,

$$p = \frac{\text{mean power dissipation}}{\dot{\psi}\,|Z|^2} \qquad \text{(C-17)}$$

The equation of a damped linear oscillator with angular amplitude η, resonant at the frequency $\Omega_0/2\pi$, and driven at $\Omega/2\pi$, is

$$\ddot{\eta} + \Omega_0^2 \eta + \frac{\gamma}{I}\dot{\eta} = \frac{\text{torque}}{I} = \frac{M_0 \cos \Omega t}{I} \qquad \text{(C-18)}$$

This is the same form as Eq. (C-13) without messy combinations of constants. By solving Eq. (C-18) and setting power equal to torque times $\dot{\eta}$, it is easily shown that

$$2p = \dot{\psi}\,\gamma \qquad \text{(C-19)}$$

To measure γ, the damping of a pendulum made of antenna wire was observed. A 5.7-lb pendulum bob was used to imitate the centrifugal force of the initial spin of Explorer I, so that the wire would have the same bending radius. The pendulum equation has the same form as

Eq. (C-18), with torque = 0, so that γ_p of the pendulum could be determined directly by fitting the solution of Eq. (C-18) to the observed motion. However, the frequency of the pendulum was the order of 1 cps, while the bending frequency of Explorer I antennas was 10 cps; and γ might depend on frequency. Therefore, γ_p was determined for pendulums of different lengths (frequencies) and extrapolated to 10 cps. It was found that p rather than γ is constant as frequency increases; which is reasonable, since this says that the same amount of energy is dissipated in bending the wire through a cycle, regardless of the speed of bending. The value found was p = 280 lb-in.^{2}/sec^2. Considerable error is introduced by not considering p as a function of tension in the wire. When Explorer I tumbled to 60 deg, the spin was reduced to one-half its original value (Eq. C-7), and the centrifugal tension which goes as ω^2 was reduced to one-fourth. This decreased tension was imitated in the laboratory by reducing the mass of the pendulum bob to one-fourth of the original 5.7 lb. This decreased p to about two-thirds of its value at 5.7 lb, which is reasonable since the wire is expected to be more conservative for a larger bending radius. Rather than attempt the integration of Eq. (C-10) with some functional form for p (θ), the constant 280 will be used in view of large errors mentioned earlier. The most interesting quantity is the time for the satellite to tumble to a certain angle. Since the tumbling starts slowly, most of the time is spent at small θ, so the constant value p(0) = 280 will be used. Finally, substituting Eq. (C-7) into Eq. (C-19) gives

$$\gamma = \frac{R}{R-1} \frac{2p}{\omega_0 \cos \theta} \tag{C-20}$$

Now the other contants in Eq. (C-16) will be listed. The basic list is as follows:

$$\begin{aligned} R &= 75 \\ c &= 21.7 \text{ in.} \\ a &= 4.0 \text{ in.} \\ \omega_0 &= 20\pi \text{ rad/sec} \\ m &= 0.0021 \text{ lb} \\ \alpha &= 1.32 \times 10^3 \text{ lb-in.}^2/\text{sec}^2 \\ \rho &= 1.75 \times 10^{-3} \text{ lb/in.} \\ I_3 &= 200 \text{ lb-in.}^2 \\ p &= 280 \text{ lb-in.}^2/\text{sec}^2 \end{aligned} \tag{C-21}$$

which determines the constants B and D:

$$\begin{aligned} B &= 0.405 \text{ lb-in.} \\ D &= 0.104 \end{aligned} \tag{C-22}$$

Substituting in Eq. (C-16) gives

$$Z = \frac{\tan \theta}{8.7 + (1.44 + i\, 0.61) \sec^2 \theta} \tag{C-23}$$

Equation (C-17) gives the quantity dT/dt needed in Eq. (C-7). It is

$$-\frac{dT}{dt} = 4 \dot{\psi} \, |Z|^2 \, p \tag{C-24}$$

The factor 4 arises since Explorer I had four antennas. Equation (C-23) gives Z, Eq. (C-7) gives $\dot{\psi}$, and Eq. (C-21) gives p. The result of substituting in Eq. (C-24) is

$$\frac{dT}{dt} = -6.94 \times 10^4 \frac{\sin^2 \theta \text{ lb-in.}^2/\text{sec}^3}{\cos \theta \left[(8.7 + 1.44 \sec^2 \theta)^2 + (0.61 \sec^2 \theta)^2\right]} \quad \text{(C-25)}$$

Substituting Eq. (C-25) in Eq. (C-10) gives

$$\frac{d\theta}{dt} = 5.35 \frac{\sin \theta \text{ min}^{-1}}{\cos^2 \theta \left[(8.7 + 1.44 \sec^2 \theta)^2 + (0.61 \sec^2 \theta)^2\right]} \quad \text{(C-26)}$$

Equation (C-26) is easily integrated to give the time τ, during which the satellite tumbles from θ_1 to θ_2. The result is

$$\tau = \left[14.1 \cos \theta + 0.456 \sec \theta - 19.2 \log_e \left(\cot \frac{\theta}{2}\right)\right]_{\theta_1}^{\theta_2} \text{ min} \quad \text{(C-27)}$$

Putting $\theta_1 = 0$ in Eq. (C-27) makes τ infinite. This is to be expected, since the antennas have a smooth ride when there is no precession at all, and no energy is dissipated; that is, $\theta = 0$ is an unstable equilibrium. The upper limit for θ_2 in Eq. (C-27) is about 60 deg since various approximations used in deriving Eq. (C-27) are invalid for larger angles.

For the case $\theta_1 = 3$ deg and $\theta_2 = 60$ deg, τ is 91 min. This agrees well with the radio intensity data for Explorer I, which shows that the satellite tumbled about this amount in one orbit around the earth. The spin appeared as an intensity variation. The frequency of this halved in one orbit, which gives $\theta_2 = 60$ deg by Eq. (C-7). Of course, θ_1 is somewhat in doubt, since Eq. (C-7) is not sensitive for small θ. The precession frequency of Eq. (C-6) also appeared on the radio record.

Since most of the time τ is spent at small angles, it is interesting to look at the approximation to Eq. (C-27) valid for small

angles. It is

$$\tau\ (\theta \text{ small}) = 19.2 \log_e \left(\frac{\theta_2}{\theta_1}\right) \text{min, or}$$

$$\theta_2 = \theta_1 \exp\left(\frac{\tau}{19.2 \text{ min}}\right) \qquad \text{(C-28)}$$

Thus, for small angles, θ increases by a factor e every 19.2 min. It is reasonable that θ should rise exponentially for small angles, because as θ increases, the antennas have a jerkier ride, increasing $|dT/dt|$, and $d\theta/dt$. Thus, θ is roughly proportional to $d\theta/dt$, the usual differential equation, that gives an exponential expression of the form Eq. (C-28).

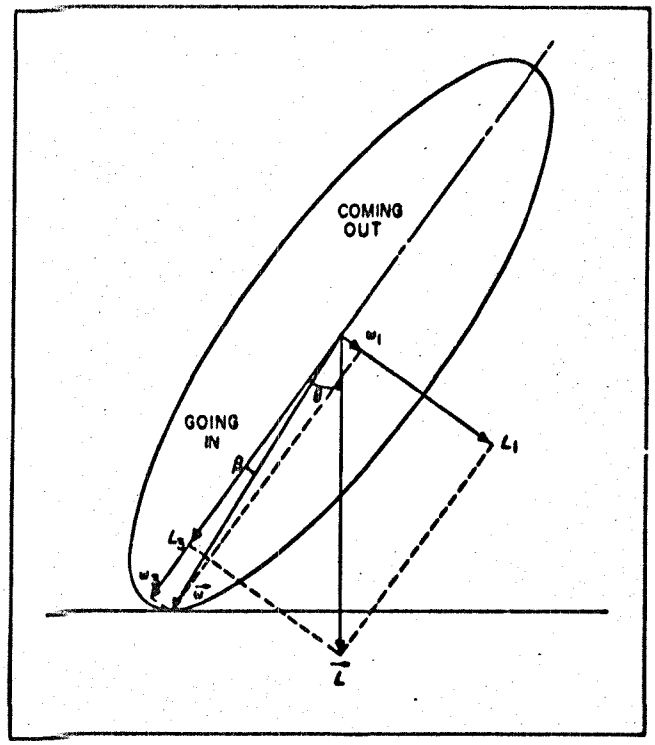

Fig. C-1. Rolling Ellipsoid of Inertia

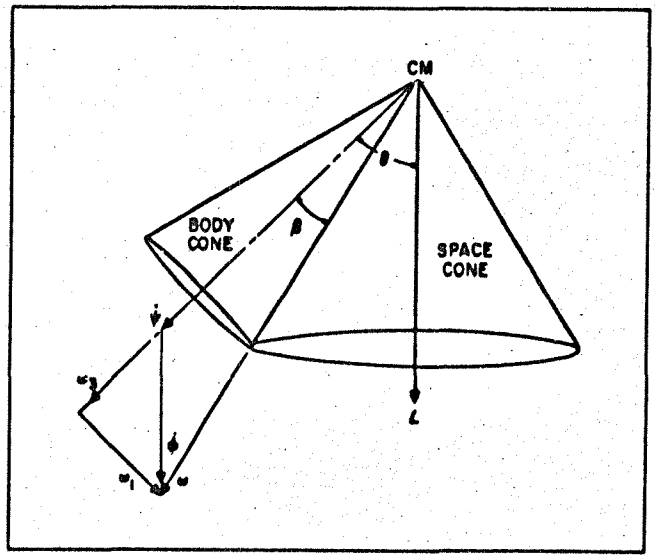

Fig. C-2. Rolling Cone Representation

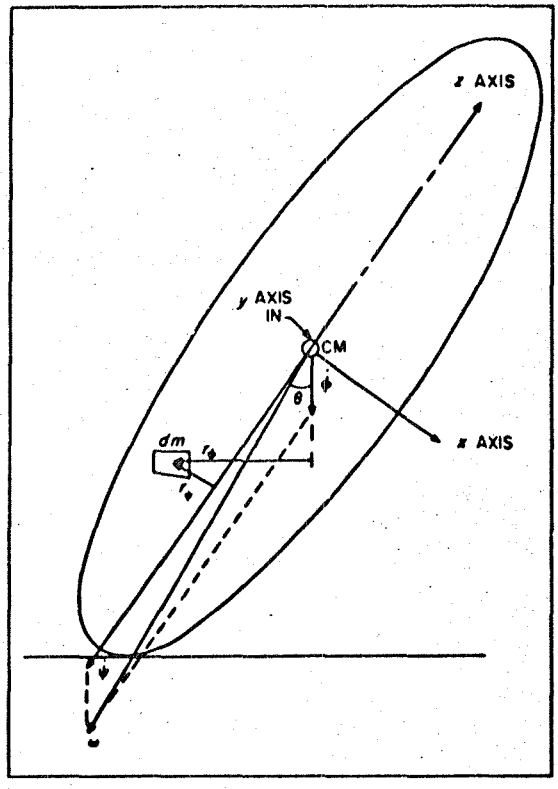

Fig. C-3. Coordinates in Ellipsoid of Inertia

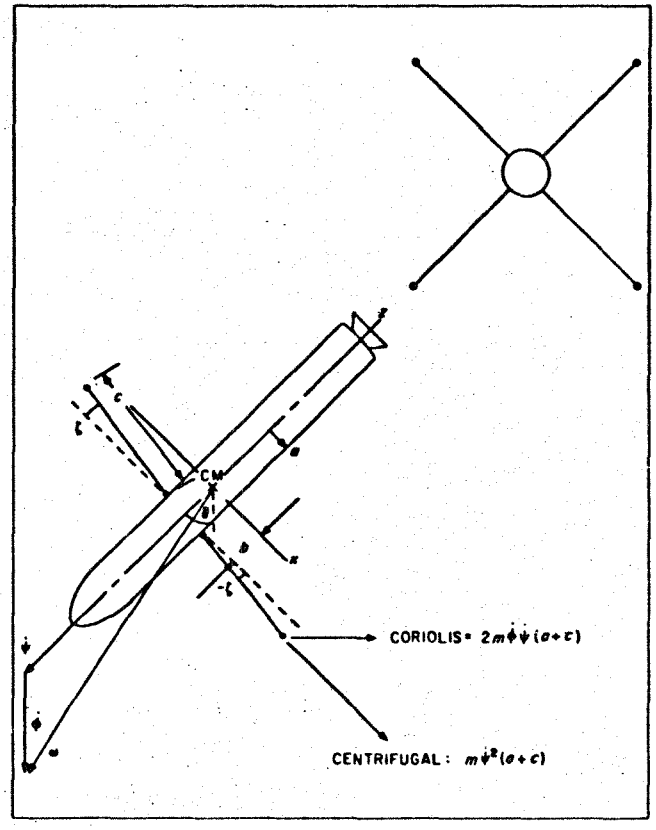

Fig. C-4. Explorer I

Appendix D. Explorer Orbital Data

	Explorer I	Explore · III	Explorer IV
Date	Feb. 1, 1958	Mar. 26, 1958	July 26, 1958
Injection time	03:55:05 GMT	17:45:06 GMT	15:06:43 GMT
Initial perigee	354 km	188 km	262 km
Initial apogee	2551 km	2793 km	2210 km
Initial period	114.95 min	115.87 min	110.21 min
Injection altitude	367 km	390 km	260 km
Injection latitude, geocentric	25.661 deg N	25.681 deg N	33.207 deg N
Injection longitude	73.050 deg W	73.060 deg W	74.696 deg W
Space-fixed injection velocity	8209.4 m/sec	8197 m/sec	8243 m/sec
Inclination angle	33.6 deg	33.4 deg	50.29 deg

REFERENCES

1. McDonald, William S., Satellite Tracking from Several Coordinated Doppler Receiving Stations, External Publication No. 554. Jet Propulsion Laboratory, Pasadena, California (to be published).
2. Goldstein, Herbert, Classical Mechanics, Addison-Wesley Press, Cambridge, 1953.
3. Slater, John C., and Frank, Nathaniel H. Mechanics, McGraw-Hill Book Co., New York, 1947.

End of Document